coatings

MDPI

Article

Application of Adaptive Neuro–Fuzzy Inference System for Forecasting Pavement Roughness in Laos

Mohamed Gharieb [1], Takafumi Nishikawa [1,*], Shozo Nakamura [1] and Khampaseuth Thepvongsa [2]

[1] Graduate School of Engineering, Nagasaki University, 1-14 Bunkyo-Machi, Nagasaki 852-8521, Japan; en.mohamed_saed@yahoo.com (M.G.); shozo@nagasaki-u.ac.jp (S.N.)
[2] Faculty of Engineering, National University of Laos, Lao-Thai Road, Sokpaluang Village, Sisatanak District, Vientiane Capital 01030, Laos; k.thepvongsa@nuol.edu.la
* Correspondence: nishikawa@nagasaki-u.ac.jp

Abstract: Laos Pavement Management System (PMS) manages 7700 km of National Roads (NRs) and estimates their Maintenance and Rehabilitation (MR) needs based on assessing pavement roughness conditions. This research aims to develop two International Roughness Index (*IRI*) models for Double Bituminous Surface Treatment (DBST) and Asphalt Concrete (AC) pavement sections using Adaptive Neuro-Fuzzy Inference System (ANFIS). A historical database of 14 years was employed for predicting the *IRI* as a function of pavement age and Cumulative Equivalent Single-Axle Load (CESAL). The optimum ANFIS structure comprises a hybrid learning algorithm with six fuzzy rules of generalized bell curve membership functions (Gbellmf) for the DBST model and nine fuzzy rules of two-sided Gaussian membership functions (Gauss2mf) for the AC model. Both models used the constant membership function for the output variable (*IRI*). The statistical evaluation results revealed that both ANFIS models (DBST and AC) have a good prediction capacity with high values of coefficient of determination (R^2 0.93 and 0.88) and low values of Mean Absolute Error (MAE 0.28 and 0.27) and Root Mean Squared Percentage Error (RMSPE 7.03 and 9.98). In addition, results revealed that ANFIS models yielded higher prediction accuracy than Multiple Linear Regression (MLR) models previously developed under the same conditions.

Keywords: *IRI*; PMS; ANFIS

Citation: Gharieb, M.; Nishikawa, T.; Nakamura, S.; Thepvongsa, K. Application of Adaptive Neuro–Fuzzy Inference System for Forecasting Pavement Roughness in Laos. *Coatings* **2022**, *12*, 380. https://doi.org/10.3390/coatings12030380

Academic Editor: Qiao Dong

Received: 6 February 2022
Accepted: 10 March 2022
Published: 14 March 2022

1. Introduction

The American Association of State Highway and Transportation Officials (AASHTO) defines a PMS as "a set of tools or methods that assist decision-makers in finding optimum strategies for providing, evaluating, and maintaining pavements in a serviceable condition over a period of time" [1]. PMS helps road authorities to optimize available funds since the total cost of pavement MR activities is usually higher than the designated budget [2]. Pavement performance prediction models are an essential component in any PMS. Successful implementation of a PMS requires accurate models for optimizing MR strategies throughout the pavement service time. Laos's road maintenance strategy is mainly based on assessing pavement roughness in terms of the *IRI* [3].

The *IRI* is defined as "the accumulated suspension vertical motion divided by the distance traveled as obtained from a mathematical model of a simulated quarter-car traversing a measured profile at 80 km/h" [4]. *IRI* is a widely employed index for assessing road users' comfort and safety [5,6]. *IRI* is generally expressed in meters per kilometer or inches per mile [7]. At present, due to its stability over time and transferability over the world, *IRI* is utilized by many highway agencies worldwide as a sound and practical index for measuring ride quality and enables the identification of MR activities [8,9].

Default Highway Development and Management (HDM-4) pavement deterioration models are currently used in Laos PMS to predict the *IRI*. HDM-4 models have been developed from the results of a large number of field experiments conducted in several

developed and developing countries. However, some factors could not be presented, either because they were not measured, would have made the model's input too complex, or their effects could not be determined within the ranges observed [10–12].

Consequently, if the HDM-4 models' equations were used without calibration, they would predict pavement conditions that may not accurately match those observed on specific road sections [13,14]. For these reasons, calibration of the HDM-4 models to local conditions is both desirable and rational [12,15]. The calibration of the HDM-4 *IRI* models requires detailed and precise distress data, for instance: initial IRI (IRI_0) value, environmental coefficient, adjusted structural number (ASN), cracking area (CR), rutting depth (RUT), and the number of potholes per km [15–17]. Such data records are not fully available for Laos yet, making it difficult to calibrate the HDM-4 *IRI* prediction models for local conditions.

2. Literature Review

Modeling via traditional regression techniques is somewhat complex and requires predefinition of the form of the regression equation. So recently, various researchers have successfully employed machine learning (ML) techniques in modeling pavement roughness and have shown satisfactory results [18–30]. ML tools are appropriate for predicting, filling, and classifying nonlinear data series. Choi et al. [23] developed an Artificial Neural Network (ANN) model to predict the *IRI* for asphalt concrete (AC) pavement sections as a function of asphalt concrete thickness (ACTH), percent passing No. 200 sieve (P_{200}), asphalt content (ASC), structural number (SN), and CESAL. Terzi [31] suggested the ANFIS approach for predicting the *IRI* of flexible pavement using the Long-Term Pavement Performance (LTPP) database. Lin et al. [19] analyzed pavement distress and *IRI*'s relationship using a back-propagation neural network.

Chou and Pellinen [25] employed the Indian PMS database to develop *IRI* models using ANN for different pavement types such as Portland cement concrete (PCC), asphalt overlay on concrete pavement, and Hot-Mix Asphalt (HMA). Nguyen et al. [22] proposed a new hybrid approach between ANFIS and various metaheuristic optimizations such as the genetic algorithm (GA), particle swarm optimization (PSO), and the firefly algorithm (FA). The proposed approach was used to develop several *IRI* hybrid models, namely GA-based ANGIS (GANFIS), PSO-based ANFIS (PSOANFIS), and FA-based ANFIS (FAANFIS). In the north of Vietnam, 2811 samples as a case study were used to validate these models. Mazari and Rodriguez [28] used a hybrid technique between ANN and Gene Expression Programming (GEP) to predict the *IRI* as a function of pavement age, CESAL, and SN. Table 1 sums up some previous studies' results that applied different ML techniques in modeling *IRI*.

The literature review of the existing *IRI* prediction models revealed that ANFIS models had a good performance in determining and predicting pavement roughness conditions over the years [22,31]. Thus, the focus of this study is to develop domestic *IRI* deterioration models using the ANFIS approach for various pavement categories to cover the influence of Laos's local conditions, which would have direct implementation without any calibration factors. Eventually, the goodness of fit of the developed ANFIS models will be compared with the MLR models previously developed under the same conditions.

Table 1. Summary of some literature *IRI* prediction models.

Authors, Year	Pavement Type	Source of Data *	Modeling *	Independent Variables *	Model Performance
Terzi, 2013 [31]	Flexible Pavement	LTPP-IMS Database	ANFIS	AGE, SN, CESAL	R^2 = 0.97
Nguyen, 2019 [22]	AC pavement	2811 Samples as a case study in the North of Vietnam	PSOANFIS	Road Length, Analysis Area, Summed Cracks, Maximum Depth of Rut, Average Depth of Rut	R = 0.888, RMSE = 0.145
			GANFIS		R = 0.872, RMSE = 0.155
			FAANFIS		R = 0.849, RMSE = 0.170
			ANN		R = 0.804, RMSE = 0.186
Chou, 2005 [25]	PCC	Indian PMS database	ANN	IRI_0, AGE, FI, AP, F/T, ESAL	R^2 = 0.98, RMSE = 0.074, N = 90
	Asphalt overlay on concrete pavement				R^2 = 0.88, RMSE = 0.124, N = 1080
	HMA				R^2 = 0.90, RMSE = 0.121, N = 640
Ziari, 2015 [27]	AC over granular base	LTPP database	ANN	AGE, AAP, AAT, AAFI, AADT, AADTT, ESAL, STH, PTH	R^2 = 0.90, RMSE = 0.09, MAPE = 5.54, N = 205
			GMDH		R^2 = 0.63, RMSE = 0.405, MAPE = 28.62, N = 205
Mazari, 2016 [28]	AC over unbound granular layers	LTPP database	Hybrid GEP-ANN	SN, AGE, CESAL	R = 0.99, RMSE = 0.049, N = 95
Georgiou, 2018 [30]	AC pavement	Direct field measurement, Greece	ANN	CR, RUT, PH	R^2 = 0.96, MAE = 6.9%, RMSPE = 8.3%
			SVM		R^2 = 0.93, MAE = 7.7%, RMSPE = 8.9%
Kaloop, 2020 [21]	JPCP	LTPP GPS-3 database	ANN	IRI_0, FI, TFAULT	r = 0.80, MAE = 0.37, RMSE = 0.49, N = 184
			WOPELM		r = 0.92, MAE = 0.23, RMSE = 0.24, N = 184

* Abbreviation definitions: AGE: Pavement age since the last overlay; PH—Potholes; TFAULT—Total Joint Faulting; ESAL—Equivalent Single-Axle Load; AADT—Average Annual Daily Traffic; AADTT—Average Annual Daily Truck Traffic; AP—Annual Precipitation; AAP—Annual Average Precipitation; FI—Freezing Index; AAFI—Annual Average Freezing Index; F/T—Number of Freeze/Thaw Cycles; AAT—Annual Average Temperature; STH—Surface Thickness; PTH—Pavement Thickness; WOPELM—Wavelet Optimally Pruned Extreme Learning Machine; SVM—Support Vector Machine; GMDH—Group Method of Data Handling; IMS—Information Management System.

3. Database and Method

3.1. Area of Study

Road pavement structure is comprised of different layers with various materials. As the material used in the surface layer could influence the progression of the *IRI*, Laos paved roads are assorted based on their structural properties into three families: DBST, AC, and Cement Concrete (CC) [32]. Laos NRs represent 13.22% of the total road network in Laos, with a total length of 7700 km. The bulk of the NRs sections is paved (85.84%), while gravel and earth sections represent only 10.70% and 3.46%, respectively [33]. Figure 1 illustrates Laos NRs classification based on construction materials.

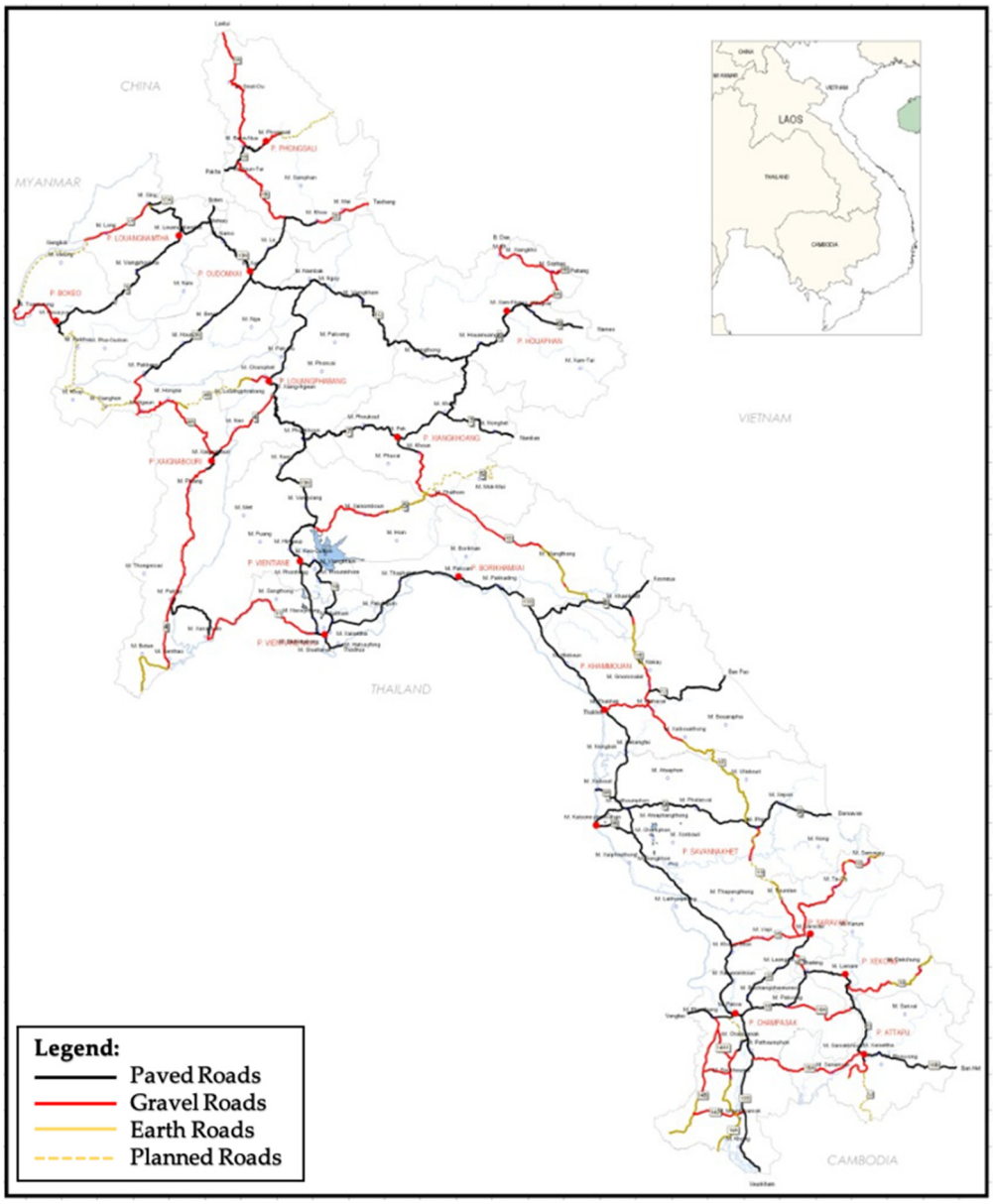

Figure 1. Laos NRs classification based on construction materials [33].

3.2. Model Variables' Description

The current study utilized the same database of the MLR models developed previously by Gharieb and Nishikawa [32]. MLR models were developed based on the Laos PMS database for the National Road Network (NRN). The original database included measurements on 214, 36, and 4 pavement sections covered DBST, AC, and CC paved NRN, respectively, over 14 years, starting from 2001 until 2015. After data screening, the valid number of sections and observations decreased. As illustrated in Figure 2, the valid observations for DBST pavement sections are only 27%. This percentage increased to be 66% for AC pavement sections and decreased to be 18% for CC pavement sections.

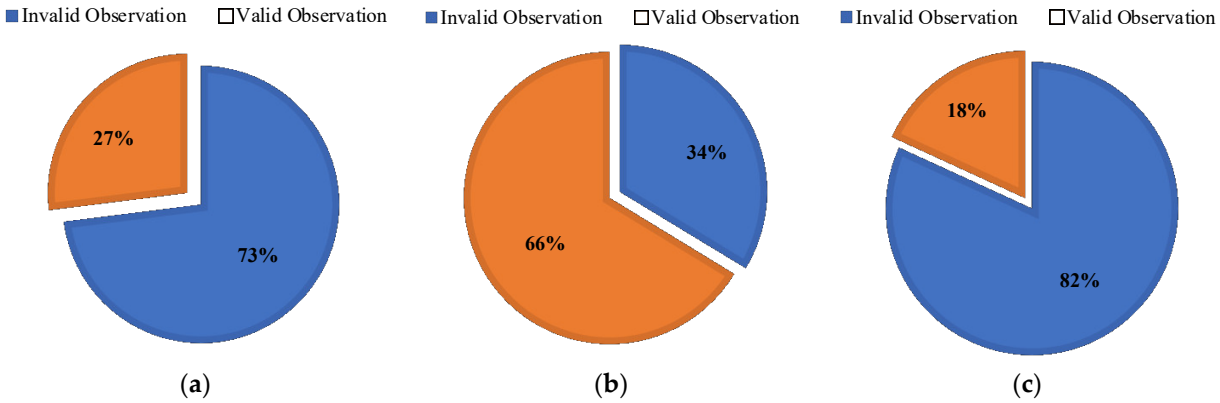

Figure 2. Percentage of valid and invalid observations for (**a**) DBST, (**b**) AC, and (**c**) CC pavement sections.

The valid number of observations for the CC surface type is only six, which is inadequate for developing a reliable model. Therefore, the analysis was limited to DBST and AC surface types. The valid observations include 269 observations from 83 sections covering 1849.26 km of DBST NRs and 122 observations from 29 sections covering 718.55 km of AC NRs [32]. Gharieb and Nishikawa [32] reported data gathering, processing, and variables' calculation efforts. MLR models were defined as shown in Equations (1) and (2).

$$IRI_{DBST} = 3.006 + 0.259\ age + 0.038\ CESAL \quad (1)$$

$$IRI_{AC} = 1.782 + 0.203\ age + 0.123\ YESAL \quad (2)$$

where:

- IRI_{DBST} is the predicted value of the *IRI* for DBST pavement sections (m/km);
- IRI_{AC} is the predicted value of the *IRI* for AC pavement sections (m/km);
- Age is the pavement age since the last overlay to the day of the *IRI* reading (years);
- CESAL is the cumulative number of equivalent single axle loads that pavement experienced from the last overlay to the day of the *IRI* reading (10^4 axles/lane);
- YESAL is the average CESAL (CESAL/Age) that pavement experienced from the last overlay to the day of the *IRI* reading (10^4 axles/lane).

Pavement Age and traffic loads (CESAL or YESAL) are used as input variables for predicting the *IRI* value. It was noticed, contrary to what is expected, that the YESAL was used in the IRI_{AC} model (Equation (2)) instead of CESAL, as was performed in the IRI_{DBST} model (Equation (1)) to avoid multicollinearity among independent variables [32].

3.3. ANFIS Approach

ANFIS is a hybrid information processing model which combines Neural Networks (NNs) and fuzzy logic [34,35]. Using learning procedures, Jang [36] suggested that ANFIS construct an input–output mapping based on the initial given fuzzy system and available input–output data pairs. Fuzzy systems and NNs are amongst the most critical soft computing methods. Fuzzy inference systems (FIS) provide a robust mechanism for knowledge representation when expert knowledge is available but does not have automated learning capabilities. NNs, on the other hand, have a robust mechanism of learning from sample data when expert knowledge is restricted but do not have knowledge representation capability.

Neuro–fuzzy hybrid systems merge the benefits of fuzzy systems for dealing with the explicit knowledge that can be defined and understood and NNs for dealing with implicit knowledge acquired by learning. Therefore, the combination of fuzzy systems and NNs addresses the constraints of both techniques and presents an outstanding data mining opportunity to solve critical and complex problems. ANFIS can accomplish a highly

nonlinear mapping and is superior to common linear methods in creating nonlinear time series [37].

NNs are used to tune fuzzy systems' membership functions (MFs), even for complicated systems. Communicating the weight of the NNs using fuzzy rules provides deep insight into the NNs, thus it is easier to design better NNs. The nonlinear MF of the neuro–fuzzy approach reduces the rule-based and saved memories, hence reducing implementation cost.

3.3.1. Fuzzy Inference Systems

Zadeh [38] suggested a fuzzy set theory in which the set boundaries were not precisely defined, but in fact, boundaries were gradational. Such a set is distinguished by a continuance of MF grades, which assigns to each object a grade of membership ranging between zero and one [37]. In classical logic, the membership value of any member is equal to 1 if it is included in the set; if not, that value is equal to 0. These kinds of sets are called "crisp sets". Conversely, the members of a fuzzy set can take the membership values ranging between 0 and 1 in fuzzy logic [39].

In the hybrid approach, the NNs are trained by data while fuzzy logic is based on linguistic rules called IF–THEN rule-based system, given by IF antecedent, THEN consequent [40]. IF–THEN rules are incorporated along with trained data to form the so-called FIS. The implementation of a FIS considers the following steps [41]:

- Fuzzification requires converting crisp or classical data into fuzzy data or MFs;
- The fuzzy inference process connects MFs with fuzzy rules to derive the fuzzy output;
- Defuzzification which calculates each associated output.

The simple FIS flowchart is illustrated in Figure 3.

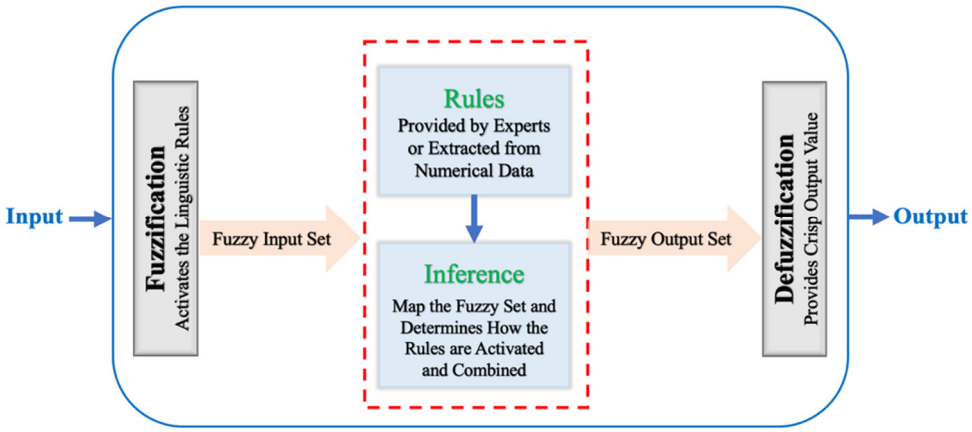

Figure 3. Simple FIS flowchart. Reprinted with permission from reference [42] Copyright 2012, Elsevier.

Three types of FIS have been widely employed in different applications: Sugeno, Tsukamoto, and Mamdani fuzzy models. The differences between the three FIS types result from the fuzzy rules that have been applied, and thus their aggregation and defuzzification procedures vary accordingly. The Sugeno system is considered more compact and computationally effective than others [43]. The consequence parameter in Sugeno FIS is either a linear equation, called first-order Sugeno FIS, or constant-coefficient, called zero-order Sugeno FIS [37].

The Sugeno model is simpler to identify because it requires fewer rules, and its parameters can be computed from numerical data using optimization methods such as least-square algorithms [44]. The advantages of the Sugeno method are that it works well with linear techniques and with optimization and adaptive techniques; it ensures continuity of the output surface, and it is computationally effective and quite convenient for mathematical analysis [45].

3.3.2. Architecture of ANFIS Model

ANFIS model structure is composed of both nodes and rules [46]. Nodes function as MFs, while rules model the relationships between inputs and outputs. In developing an ANFIS model, eight different types of MFs could be considered. These types are: triangular MF (Trimf), trapezoidal MF (Trapmf), Gbellmf, Gaussian curve MF (Gaussmf), Gauss2mf, pi-shaped curve MF (Pimf), the composed difference between two sigmoidal MFs (Dsigmf), and the product of two sigmoid MFs (Psigmf) [47].

ANFIS requires feature extraction rules applied to the input-target data stocked in a fuzzy-based rule system (i.e., 'the IF-THEN' rule). The rules are defined based on their antecedents (If part) and consequents (Then part). As shown in Figure 4a, two fuzzy IF-THEN rules are considered to present the ANFIS architecture based on a first-order Sugeno model. Two fuzzy IF-THEN rules are defined as follows:

$$\text{Rule}_{(1)}\text{: If "x" is } A_1 \text{ and "y" is } B_1\text{, Then: } f_1 = p_1 \times x + q_1 \times y + r_1;$$

$$\text{Rule}_{(2)}\text{: If "x" is } A_2 \text{ and "y" is } B_2\text{, Then: } f_2 = p_2 \times x + q_2 \times y + r_2.$$

where:

- x and y are the inputs;
- A_i and B_i are fuzzy sets;
- f_i is the output within the fuzzy region specified by the fuzzy rule;
- p_i, q_i, and r_i are the design parameters that are determined during the training process.

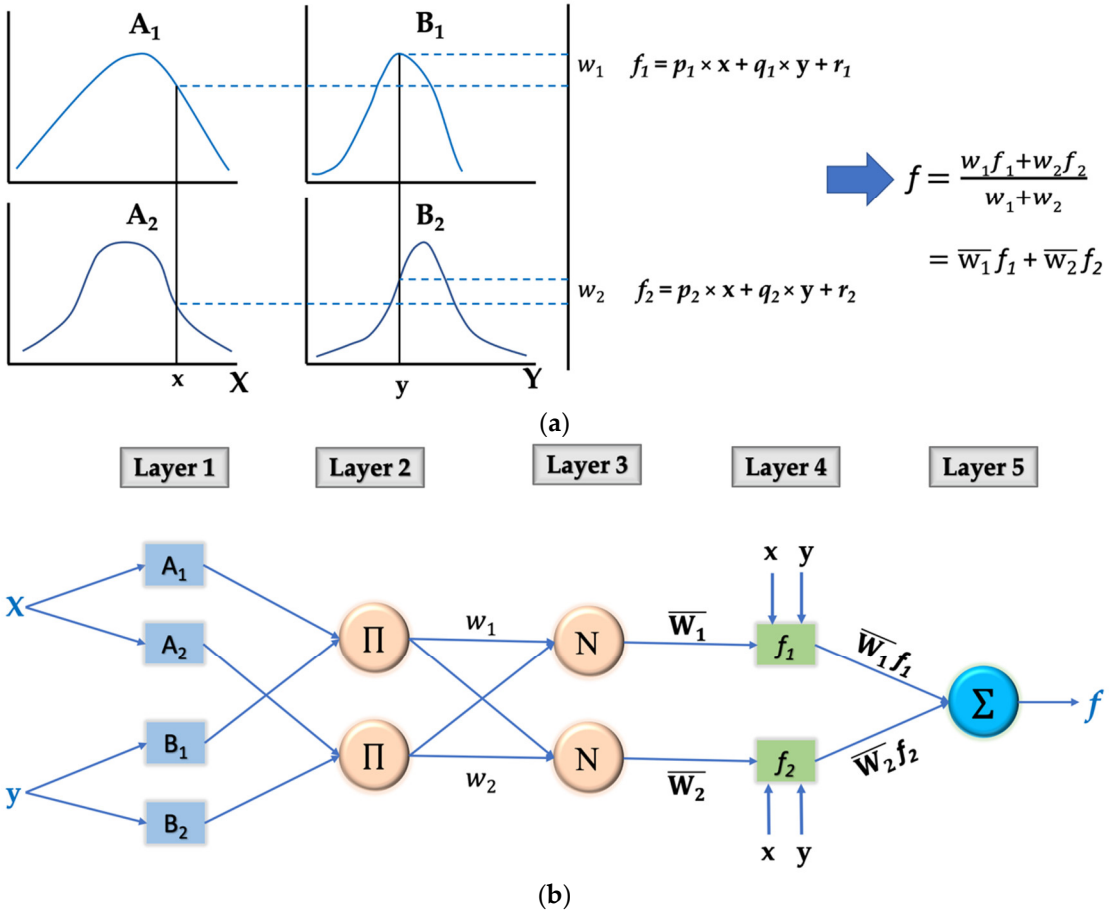

Figure 4. (**a**) A first-order Sugeno fuzzy model, (**b**) typical ANFIS architecture. Reprinted with permission from reference [31] Copyright 2013, Elsevier.

ANFIS model consists of five layers or phases comprised of (1) fuzzification, (2) the rules phase, (3) the normalization phase, (4) the defuzzification phase, and (5) the overall output phase (Figure 4b). A brief description of the role of these layers is described in detail following [37].

Layer 1 is the fuzzification layer in which all nodes are adaptive. The outputs of layer 1 are inputs MFs, which are given by the following equations:

$$\begin{array}{c} O_{1,i} = \mu_{Ai}\,(x),\ i = 1,2, \\ O_{1,i} = \mu_{Bi-2}\,(y),\ i = 3,4, \end{array} \quad (3)$$

where x and y are the crisp inputs to node i, A_i and B_i are the linguistic labels characterized by the proper MFs μ_A and μ_B, respectively.

In layer 2, nodes are fixed nodes labeled by π, indicating that they perform as a simple multiplier. The firing strength of the rules (ω_i) is determined as given in Equation (4), for which the resulting values of the previous layer are multiplied, giving adjusted nodes. Each node represents the firing strength of each rule.

$$O_{2,i} = \omega_i = \mu_{Ai}\,(x) \times \mu_{Bi}\,(y),\ i = 1,\ 2. \quad (4)$$

In layer 3, nodes are also fixed nodes labeled by N to indicate that they play a normalization role in the firing strength from the previous layer. This layer output can be computed as follows:

$$O_{3,i} = \varpi_i = \frac{\omega_i}{\omega_1 + \omega_2},\ i = 1,\ 2. \quad (5)$$

In layer 4, nodes are adaptive. The result of the previous layer is multiplied by multiple linear equations, which represent the rule systems of the Sugeno fuzzy model. This layer output is given by:

$$O_{4,i} = \varpi_i\ f_i = \varpi_i\,(p_i\,x + q_i\,y + r_i),\ i = 1,\ 2. \quad (6)$$

where ϖ_i is the output of layer three and $\{p_i, q_i, r_i\}$ are the parameter set. Parameters in this layer are referred to as consequent parameters.

Layer 5 is the output layer in which the single node computes the overall output by summing all the rules from the previous layer. Accordingly, the defuzzification process transforms each rule's fuzzy results into a crisp output in this layer. The overall output is calculated as in Equation (7).

$$O_{5,i} = \sum_i \varpi_i f_i = \frac{\sum_i\ \omega_i\ f_i}{\sum_i\ \omega_i} \quad (7)$$

3.3.3. Hybrid Learning Algorithm

MFs parameters are adjusted in learning cycles that can employ either a hybrid or a back-propagation learning algorithm. The hybrid algorithm incorporates the back-propagation and Least Square Error (LSE) [48]. It uses a two-pass learning cycle, a forward and a backward pass. The LSE algorithm adjusts the consequent parameters in fuzzy rules in the forward pass.

In the backward pass, the premise parameters of the rules are adjusted using a back-propagation algorithm (usually Gradient Descent) [49]. Rule complexity depends on the number of input variables and the number of values in term sets. It has been proven that this hybrid algorithm is powerfully effective in training ANFIS [37].

3.4. Model Assessment Criteria

Model results will be evaluated using many statistical checks. R^2 will assess the relationship between the predicted and observed values. R^2 is computed using the following equation [50]:

$$R^2 = 1 - \frac{\sum_{i=1}^{n}\left(IRI_{i,act} - IRI_{i,pred}\right)^2}{\sum_{i=1}^{n}(IRI_{i,act} - \overline{IRI}_{act})^2} \quad (8)$$

In Equation (8), n is the number of samples, IRI_{act} and IRI_{pred} are the actual and the predicted *IRI* value, respectively, $\overline{IRI}_{act}$ is the average value of the actual *IRI*. The range of R^2 values 0–1, with 1 being the highest precise relationship possible.

Other assured statistical checks, such as MAE and the RMSPE, were also utilized to assess the accuracy of the proposed model. MAE and RMSPE mathematical expressions are denoted by Equations (9) and (10) as follows [50]:

$$\text{MAE} = \frac{1}{n}\sum_{i=1}^{n}\left|IRI_{i,act} - IRI_{i,pred}\right| \quad (9)$$

$$\text{RMSPE} = \sqrt{\frac{1}{n}\sum_{i=1}^{n}\left(\frac{IRI_{i,act} - IRI_{i,pred}}{IRI_{i,act}}\right)^2} \quad (10)$$

A good prediction model should have a high R^2 and low MAE and RMSPE. The percentage relative error (RE%) was also utilized to evaluate the accuracy of the developed model. Equation (11) shows the mathematical expression for the calculation of RE% [47].

$$\text{RE\%} = \left(\frac{IRI_{i,act} - IRI_{i,pred}}{IRI_{i,act}}\right) \times 100\% \quad (11)$$

4. ANFIS Model Development

ANFIS approach utilized the Laos PMS database to develop an ANFIS model for each type of pavement. Data points were randomly divided into training (70%), checking (15%), and testing (15%) datasets. The collected data were statistically analyzed to check the consistency and reliability. The descriptive statistics of variables used for training, checking, testing, and all datasets in both DBST and AC models are summarized in Table 2.

Table 2. Descriptive statistics of the variables used for *IRI* modeling.

Variable	Training (70%)				Checking (15%)				Test (15%)				All Data			
	Min	**Max**	**Mean**	**Std**	**Min**	**Max**	**Mean**	**Std**	**Min**	**Max**	**Mean**	**Std**	**Min**	**Max**	**Mean**	**Std**
DBST Model																
Age	0.10	13.39	5.50	3.76	0.11	12.53	7.25	3.60	1.58	14.10	7.27	3.22	0.10	14.10	6.03	3.73
CESAL	0.02	99.26	12.44	15.71	0.07	56.25	12.79	13.52	0.25	87.07	17.75	22.03	0.02	99.26	13.28	16.55
IRI	2.28	8.83	4.92	1.42	2.20	8.12	5.43	1.46	3.49	8.91	5.53	1.39	2.20	8.91	5.09	1.44
AC Model																
Age	0.09	13.08	5.81	3.37	0.09	11.76	6.09	3.69	0.18	11.53	6.44	3.66	0.09	13.08	5.95	3.44
YESAL	0.03	13.15	4.24	3.00	0.15	15.13	4.87	3.65	0.61	20.53	4.85	4.55	0.03	20.53	4.42	3.34
IRI	1.47	5.46	3.47	0.99	1.90	5.17	3.71	1.06	1.87	5.31	3.67	1.12	1.47	5.46	3.54	1.02

The database covers a wide range of pavement conditions under different traffic loading characteristics, which raises confidence in the developed models. The training data are used to fit the model, while the checking data are used to avoid overfitting. The test data are used to compute the quality of the prediction estimates.

ANFIS models were developed using the MATLAB Fuzzy Logic Toolbox (FLT, R2020b) from MathWorks. This tool helps construct and evaluate fuzzy systems using a graphical user interface. It consists of an MF editor, a FIS editor, the rule editor, the fuzzy inference

viewer, and the output surface viewer. The MF editor displays and edits the MFs associated with all input and output variables. The FIS editor displays general information about a FIS. The rule editor allows the user to construct the rule statements. The rule viewer enables users to interpret the entire fuzzy inference process at once [51].

There is no standard method for selecting the appropriate ANFIS structure, so training the ANFIS model with various types and numbers of MFs, different rules, and epoch numbers, and then selecting the structure that achieves minimum RMSE was employed [22]. As an initial guess, two MFs were used for each input (2–2). Then, a trial network with varying types of MFs (8 types) was tested to compare their abilities in modeling the *IRI*. Table 3 presents the resulting error (RMSE) of different network architectures using various numbers and types of MFs for training, checking, testing, and overall datasets of DBST and AC models, respectively.

Table 3. Performance of different models under various MF numbers and types for DBST and AC pavement sections.

DBST Model						AC Model					
MF No.	MF Type	Root Mean Squared Error (RMSE)				MF No.	MF Type	Root Mean Squared Error (RMSE)			
		Training	Checking	Testing	Overall			Training	Checking	Testing	Overall
2–2	Trimf	0.440	0.541	0.448	0.456	2–2	Trimf	0.382	0.237	0.405	0.364
	Trapmf	0.518	0.671	0.557	0.546		Trapmf	0.404	0.228	0.468	0.387
	Gbellmf	0.480	0.607	0.478	0.498		Gbellmf	0.399	0.230	0.466	0.384
	Gaussmf	0.442	0.539	0.432	0.455		Gaussmf	0.396	0.227	0.433	0.377
	Gauss2mf	0.436	0.577	0.445	0.458		Gauss2mf	0.388	0.235	0.467	0.377
	Pimf	0.664	0.804	0.673	0.686		Pimf	0.447	0.279	0.498	0.430
	Dsigmf	0.627	0.757	0.575	0.638		Dsigmf	0.418	0.246	0.480	0.402
	Psigmf	0.627	0.757	5.696	1.400		Psigmf	0.425	0.246	0.485	0.407
3–3	Trimf	0.405	0.502	0.408	0.420	3–3 *	Trimf	0.375	0.224	0.578	0.383
	Trapmf	0.400	0.498	1.365	0.558		Trapmf	0.439	0.442	0.678	0.474
	Gbellmf	0.458	0.590	0.524	0.487		Gbellmf	0.399	0.320	0.471	0.397
	Gaussmf	0.367	0.477	0.355	0.382		Gaussmf	0.382	0.265	0.432	0.372
	Gauss2mf	0.408	0.551	0.410	0.430		Gauss2mf **	0.355	0.264	0.439	0.354
	Pimf	0.463	0.601	0.483	0.486		Pimf	0.472	0.472	0.705	0.507
	Dsigmf	0.428	0.556	0.641	0.479		Dsigmf	0.446	0.430	0.550	0.459
	Psigmf	0.429	0.558	0.709	0.490		Psigmf	0.446	0.430	0.550	0.459
2–3	Trimf	0.438	0.530	0.434	0.451	2–3	Trimf	0.378	0.232	0.584	0.387
	Trapmf	0.497	0.606	0.517	0.516		Trapmf	0.447	0.243	0.570	0.435
	Gbellmf	0.495	0.607	0.521	0.516		Gbellmf	0.410	0.230	0.422	0.385
	Gaussmf	0.501	0.599	0.502	0.516		Gaussmf	0.396	0.225	0.419	0.374
	Gauss2mf	0.631	0.736	0.646	0.649		Gauss2mf	0.400	0.238	0.414	0.378
	Pimf	0.620	0.756	0.658	0.646		Pimf	0.441	0.247	0.572	0.432
	Dsigmf	0.594	0.711	0.539	0.603		Dsigmf	0.428	0.244	0.418	0.399
	Psigmf	0.589	0.709	0.542	0.600		Psigmf	0.426	0.244	0.418	0.398
3–2 *	Trimf	0.380	0.488	0.391	0.397	3–2	Trimf	0.384	0.226	0.383	0.361
	Trapmf	0.469	0.575	0.523	0.492		Trapmf	0.370	0.271	0.474	0.371
	Gbellmf **	0.357	0.449	0.363	0.372		Gbellmf	0.405	0.245	0.459	0.389
	Gaussmf	0.382	0.493	0.359	0.395		Gaussmf	0.398	0.232	0.417	0.376
	Gauss2mf	0.412	0.488	0.422	0.425		Gauss2mf	0.389	0.245	0.456	0.378
	Pimf	0.526	0.685	0.558	0.554		Pimf	0.441	0.308	0.545	0.437
	Dsigmf	0.458	0.611	0.490	0.485		Dsigmf	0.371	0.257	0.444	0.365
	Psigmf	0.465	0.625	0.499	0.494		Psigmf	0.367	0.258	0.440	0.362
4–4	Trimf	0.384	0.446	0.385	0.394	4–4	Trimf	0.362	0.263	0.582	0.379
	Trapmf	0.463	0.500	0.912	0.535		Trapmf	0.363	0.248	0.627	0.385
	Gbellmf	0.415	0.466	0.532	0.440		Gbellmf	0.350	0.310	0.457	0.360
	Gaussmf	0.397	0.543	0.451	0.427		Gaussmf	0.348	0.386	0.439	0.367
	Gauss2mf	0.459	0.513	7.188	1.468		Gauss2mf	0.357	0.246	0.658	0.385
	Pimf	0.495	0.555	1.219	0.611		Pimf	0.362	0.254	0.629	0.385
	Dsigmf	0.456	0.509	4.497	1.065		Dsigmf	0.357	0.245	0.763	0.400
	Psigmf	0.456	0.509	4.497	1.065		Psigmf	0.357	0.245	0.863	0.415
5–5	Trimf	0.359	0.419	0.632	0.408	5–5	Trimf	0.328	0.278	0.887	0.403
	Trapmf	0.384	0.464	0.754	0.451		Trapmf	0.321	0.344	0.908	0.411
	Gbellmf	0.366	0.425	12.739	2.215		Gbellmf	0.302	0.300	0.924	0.393
	Gaussmf	0.360	0.421	4.438	0.976		Gaussmf	0.305	0.278	1.000	0.403
	Gauss2mf	0.385	0.449	0.738	0.447		Gauss2mf	0.320	0.412	1.433	0.498
	Pimf	0.400	0.466	0.789	0.467		Pimf	0.335	0.548	0.630	0.410
	Dsigmf	0.382	0.445	0.514	0.411		Dsigmf	0.318	0.379	1.043	0.433
	Psigmf	0.382	0.445	0.514	0.411		Psigmf	0.318	0.379	1.043	0.433

* The optimum number of MFs, ** The optimum MF type.

The optimum MF numbers were (3–2) for the DBST model and (3–3) for the AC model, which gave the lowest modeling errors in all the datasets. In modeling the *IRI* for DBST, the Gbellmf gave the lowest errors in all the datasets other than MF types. Meanwhile, for AC, the Gauss2mf showed the lowest modeling errors for training, checking, testing, and overall datasets. After determining the optimum number and type of MF, Figure 5 displays the architecture of the proposed ANFIS models for the DBST and the AC pavement sections.

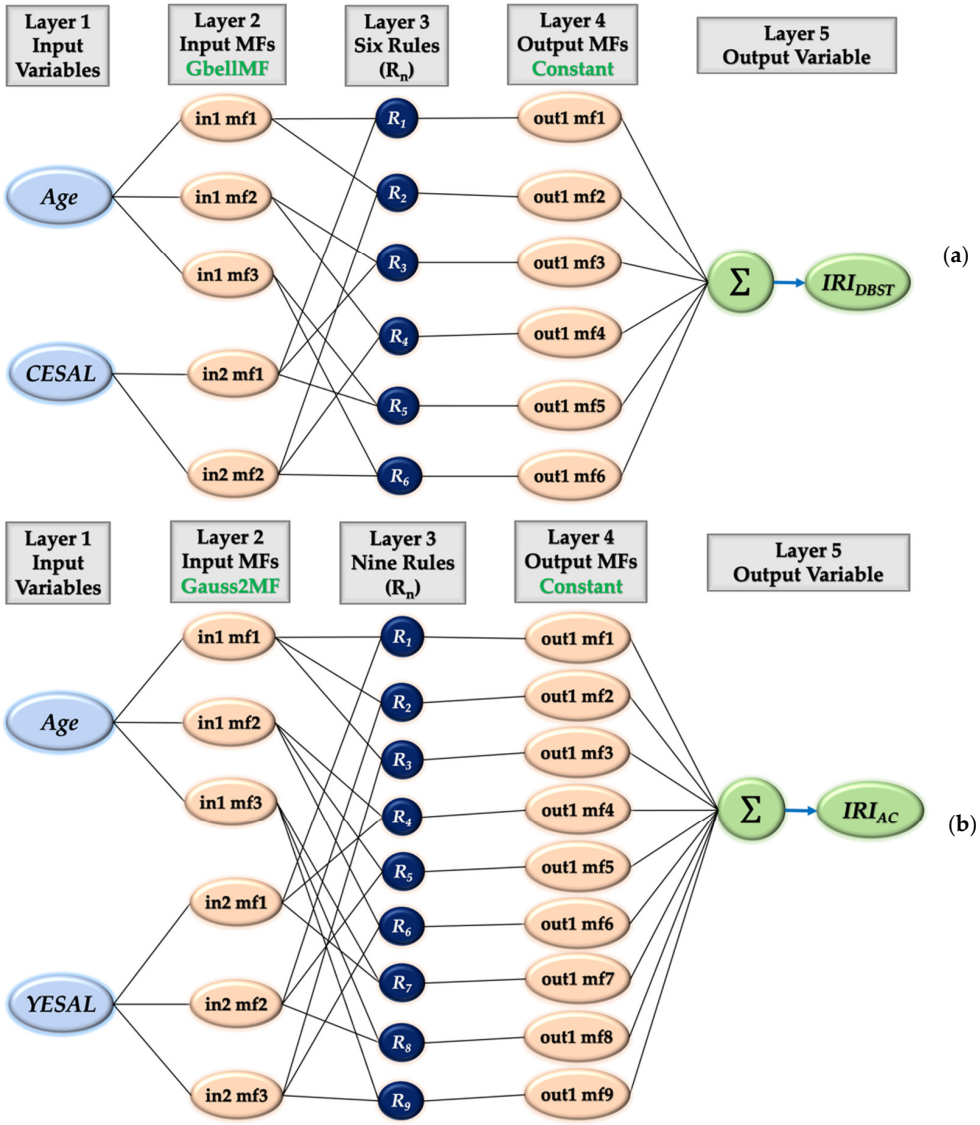

Figure 5. ANFIS model structure for the (**a**) DBST and (**b**) AC pavement sections.

The selection of the optimum epoch number is a very significant factor in ANFIS modeling. Increasing the epoch number does not always mean enhancing the performance of ANFIS modeling. Usually, the modeling errors decrease by increasing the epoch number to a point, and then the errors increase afterward. Identifying this point is a necessity in ANFIS modeling.

Figure 6 illustrates the error performance versus epochs to check the progress while training and checking the proposed model. Epochs are the number of learning cycles where rules were adjusted to minimize the difference between the measured and the predicted *IRI*.

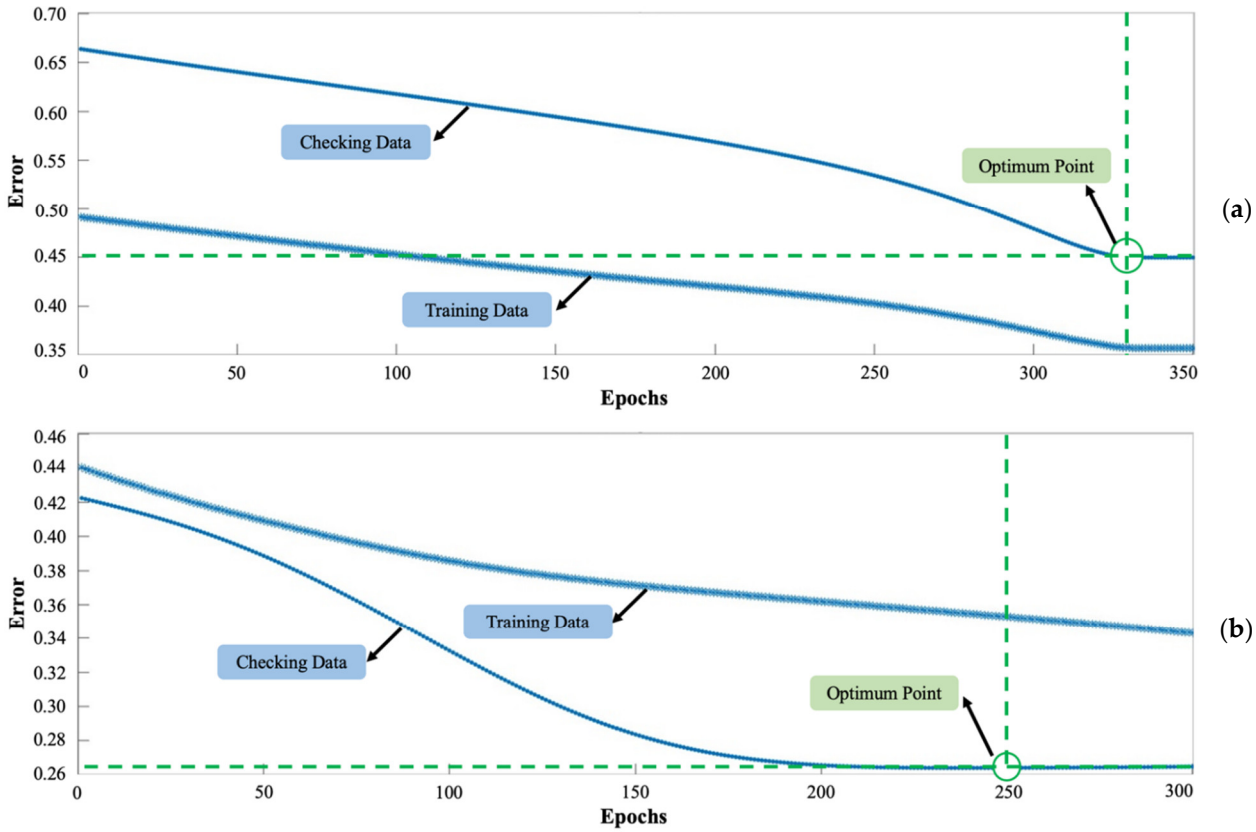

Figure 6. ANFIS error performance while training and checking for the (**a**) DBST model and (**b**) AC model.

The error function in terms of RMSE between the measured and predicted *IRI* values were monitored during the training process. When the network began to overfit the data, the error on the checking set began to increase, so the training was stopped at the optimum number of epochs at the minimum of the checking set error. The results revealed that the RMSE decreases with the training epochs. For DBST pavement sections, the best training performance of the model is gained at epoch 335, where the checking error is equal to 0.493. At the same time, the best training performance of the AC model is achieved at epoch 250, where the checking error is equal to 0.264. These epoch numbers give the lowest modeling errors and avoid the model's overfitting problem.

The initial and final Gbellmf plots for input variables (AGE and CESAL) for the DBST model are illustrated in Figures 7 and 8. As shown in Figure 7, there are three MFs for the AGE input and two MFs for the CESAL input. After both input models have been trained using the ANFIS approach, the final MFs, as shown in Figure 8, provide better interpretability than the initial one.

The initial and final Gauss2mf plots for input variables (AGE and YESAL) for the AC model are also shown in Figures 9 and 10. There are three MFs for both inputs (AGE and YESAL). As shown in Figure 10, the final MFs provide better interpretation than the initial one (Figure 9) after both input models have been trained using the ANFIS methodology.

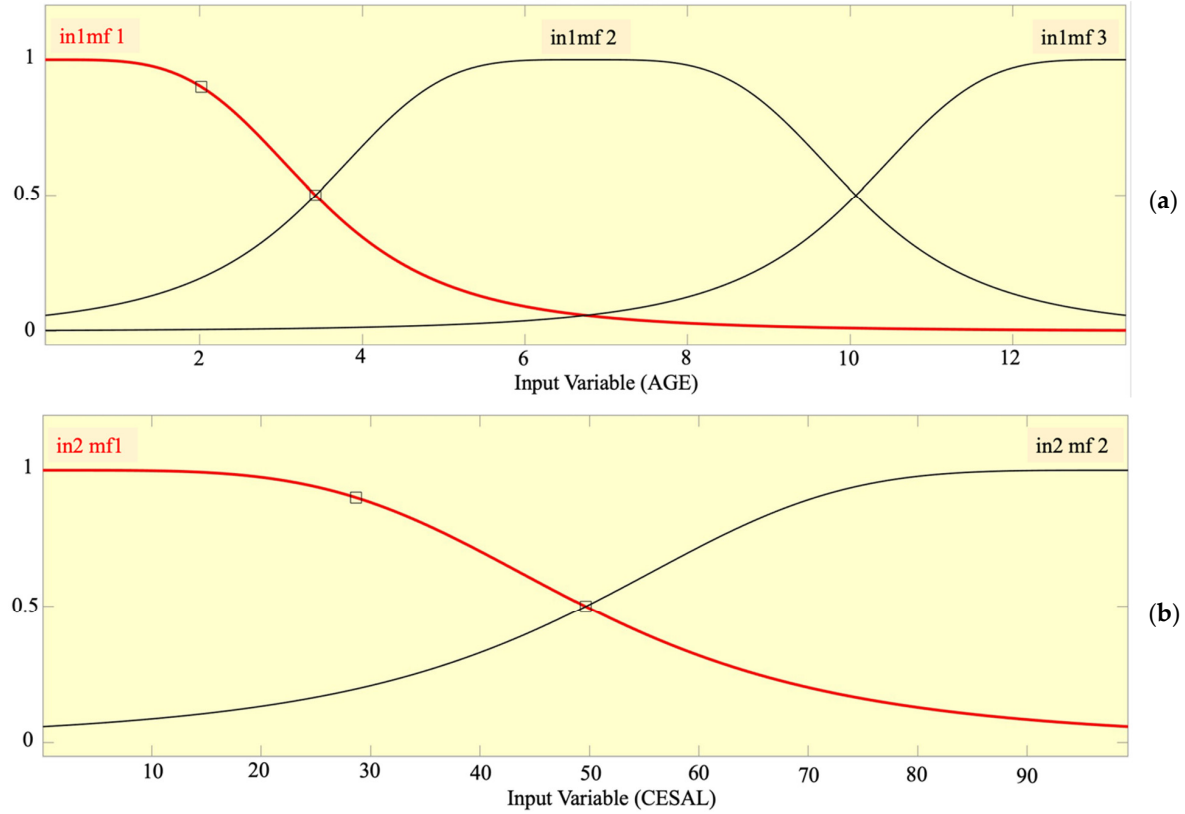

Figure 7. Initial MFs for DBST input variables of (**a**) AGE and (**b**) CESAL.

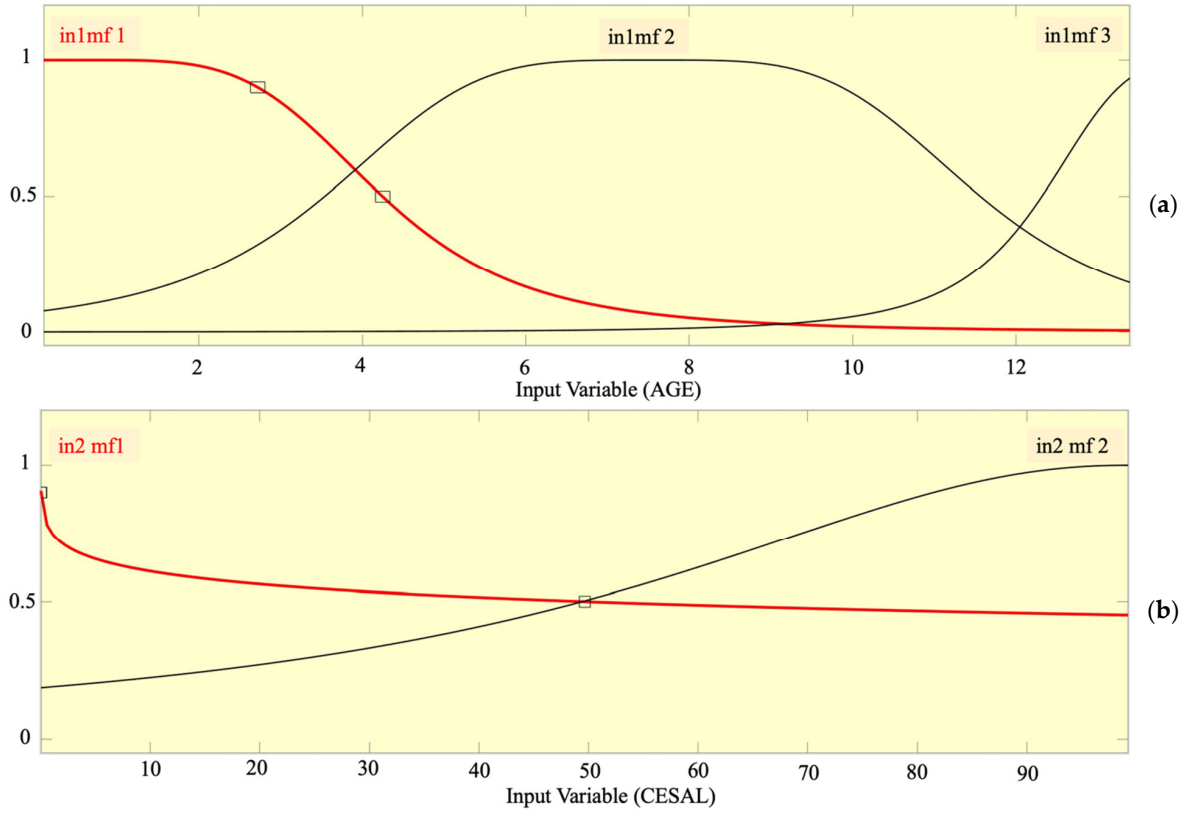

Figure 8. Final MFs for DBST input variables of (**a**) AGE and (**b**) CESAL.

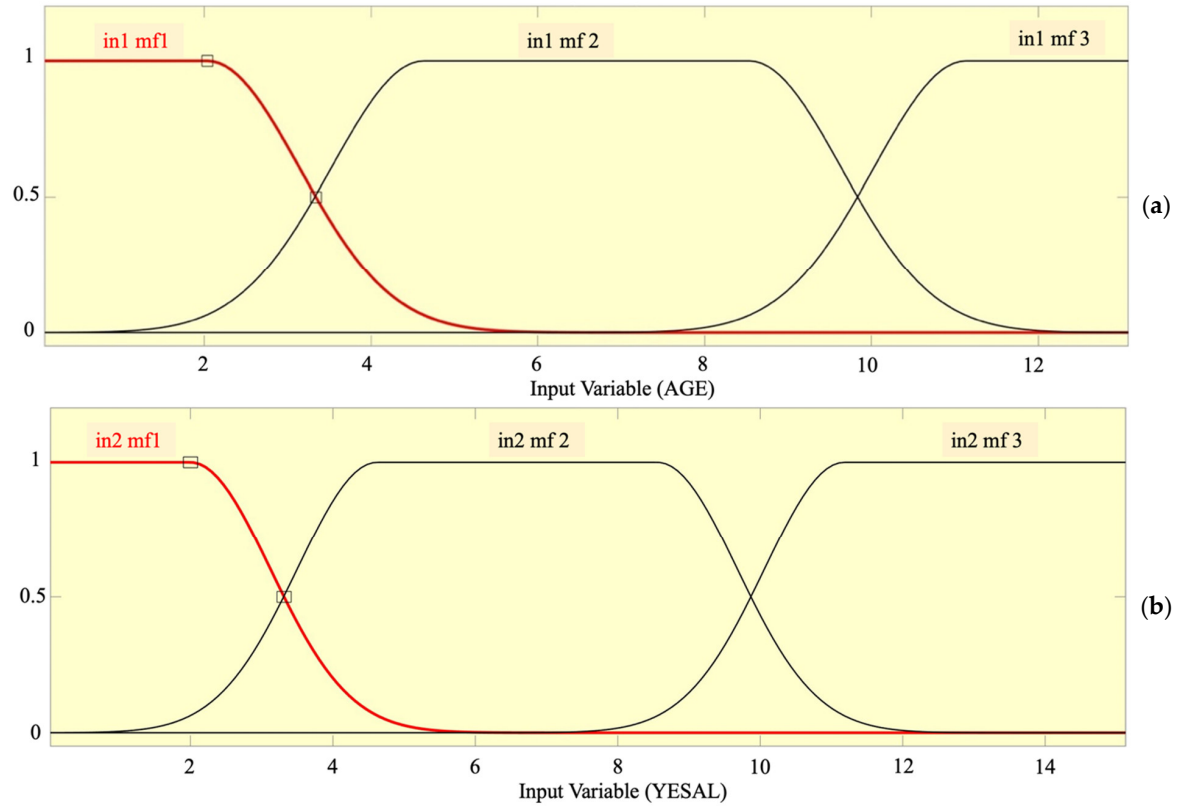

Figure 9. Initial MFs for AC input variables of (**a**) AGE and (**b**) YESAL.

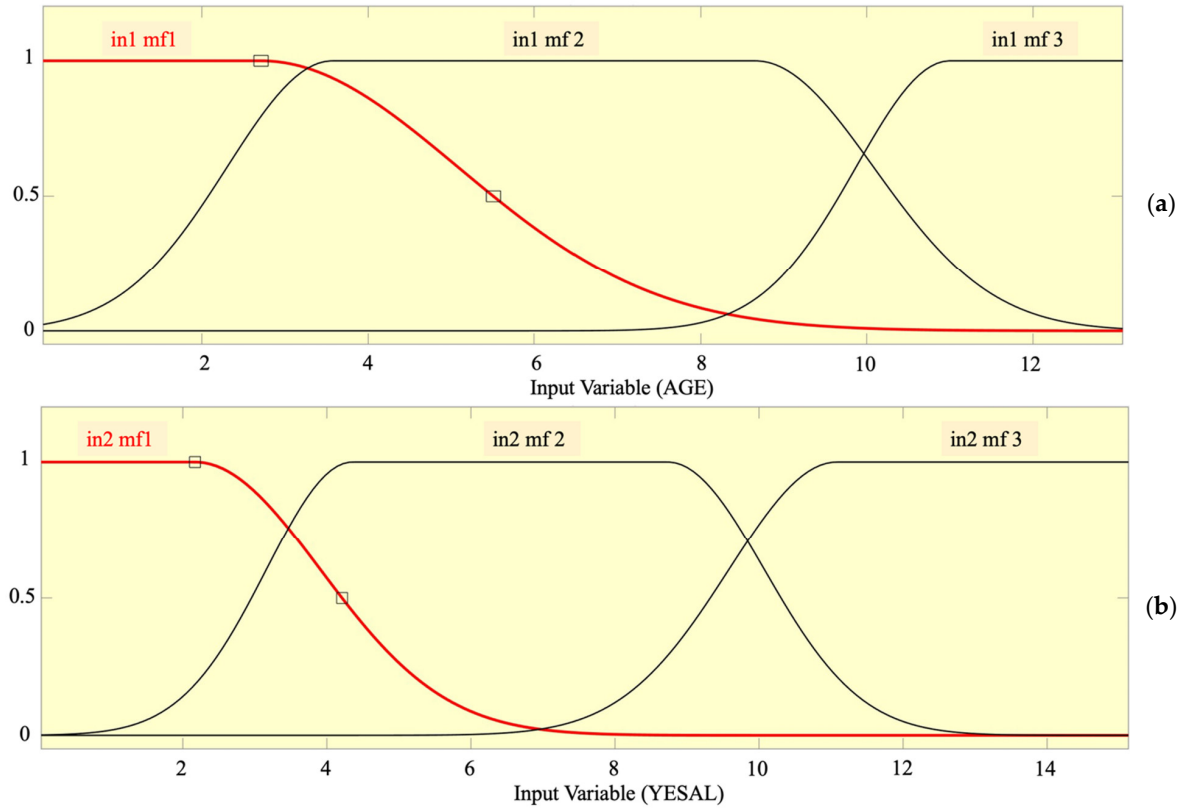

Figure 10. Final MFs for AC input variables of (**a**) AGE and (**b**) YESAL.

The comparison between the measured and the predicted *IRI* values for training, checking, and testing data sets in both DBST and AC models developed are illustrated in Figures 11 and 12. The modeling outputs show an excellent performance where the two lines (ANFIS *IRI* and Measured *IRI*) are almost parallel with some minor differences in both models.

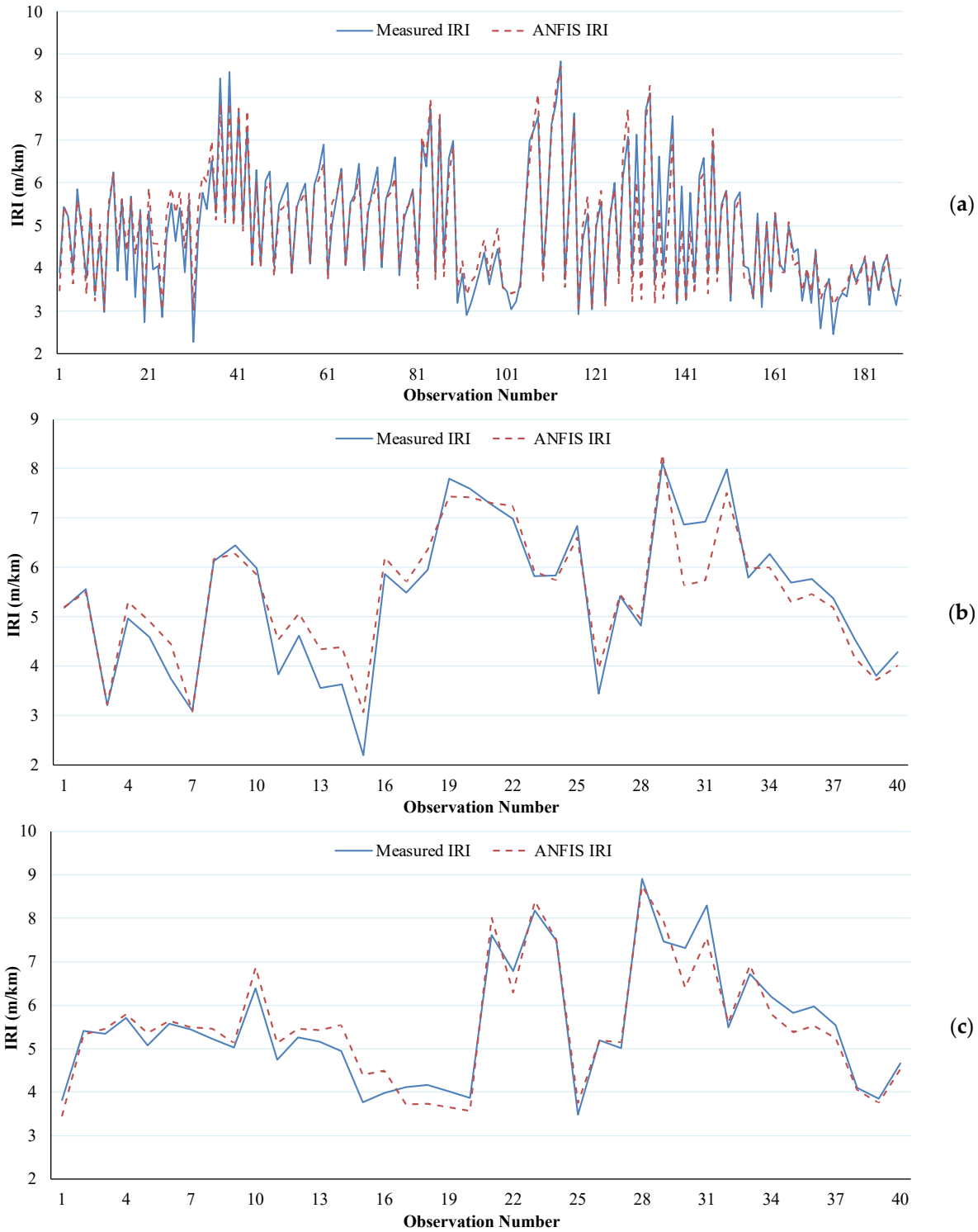

Figure 11. Comparison between the measured and the modeled *IRI* values of the DBST model for the (**a**) training, (**b**) checking, and (**c**) testing data sets.

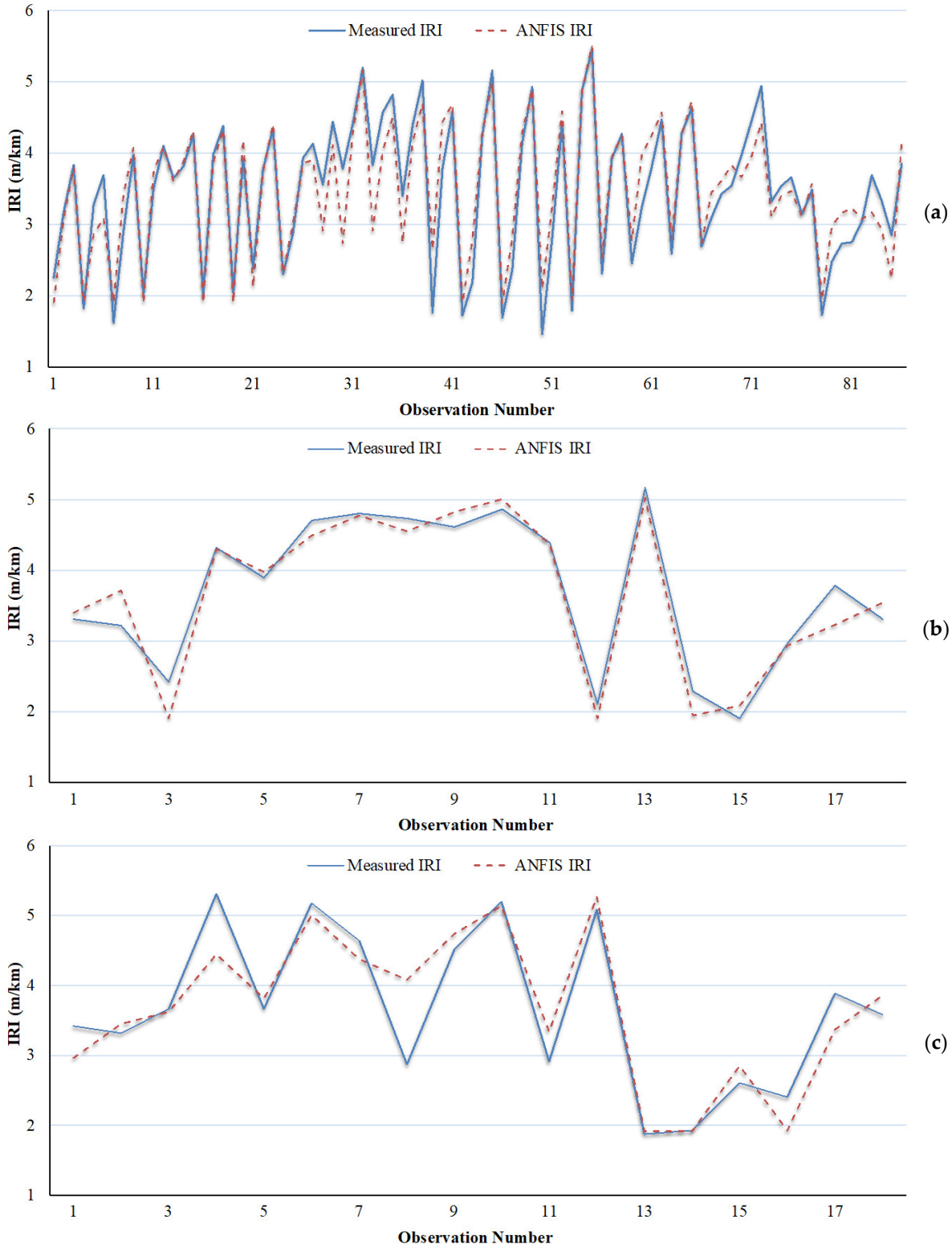

Figure 12. Distribution of the measured and the predicted *IRI* values of the AC model for the (**a**) training, (**b**) checking, and (**c**) testing data sets.

Figure 13 demonstrates the assigned rules in the optimum ANFIS model structure for modeling DBST and AC, respectively. In Figure 13a, the results of the optimum ANFIS structure for the DBST model are illustrated in the rule viewer. The first column of the rule viewer represents the change rate of pavement age, and the second column represents the change rate of CESAL. The third column is for output, which represents the changes of *IRI*.

The input values in the rule viewer can be set manually in the fuzzy logic toolbox to check rule set is working according to requirements and system accuracy. The input values (6.75, 49.6) are entered related to fuzzy sets, and decision rules are applied. The fuzzy result of the output variable (*IRI*) is 7.00, which is the highest chance of pavement roughness condition.

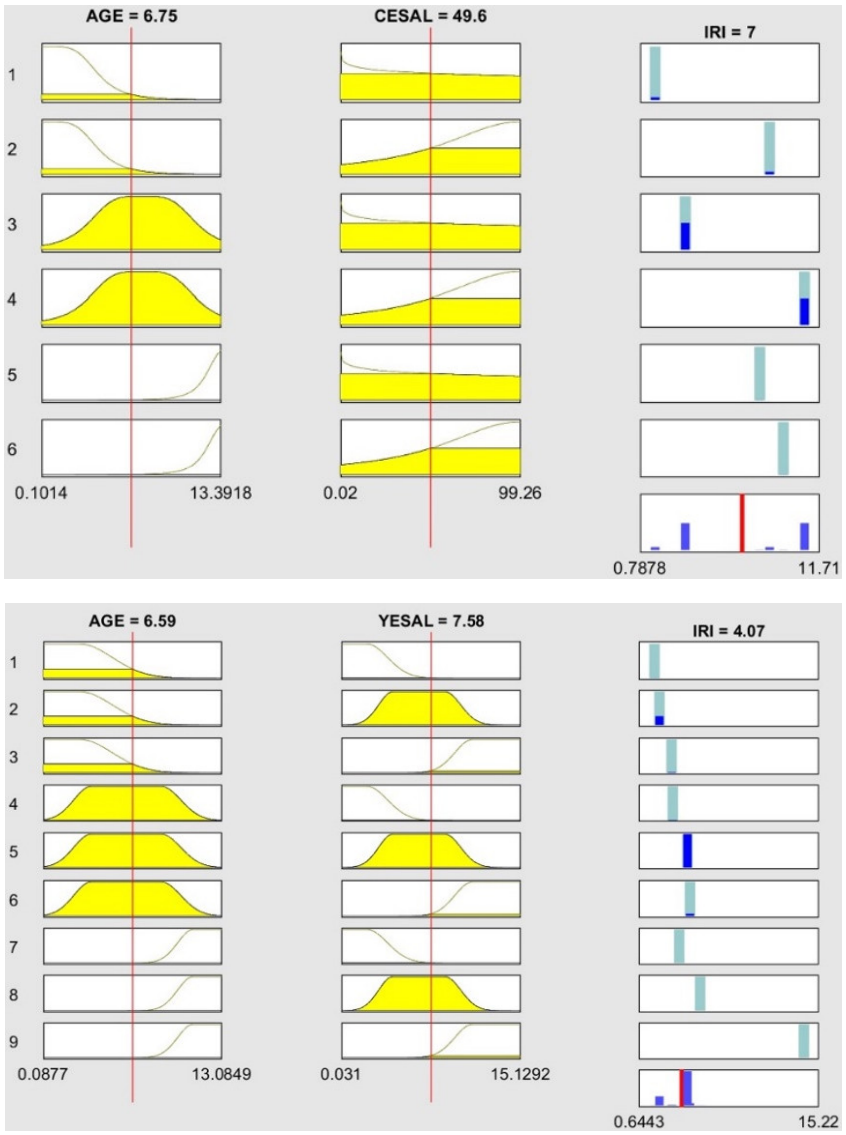

Figure 13. The rules of the optimum ANFIS structure for the (**a**) DBST model and (**b**) AC model.

In Figure 13b, the results of the optimum ANFIS structure for the AC model are shown in the rule viewer. The first column represents pavement age, which means how much pavement age is changed, and its value is set by 6.59. The second column represents YESAL, which indicates how much traffic loads are changed within defined pavement age, and its value is set by 7.58. The third column represents the output value of *IRI* (4.07), which is evaluated by input values and according to rule sets.

The full descriptions of the final ANFIS models in modeling the *IRI* for DBST and AC pavement sections are listed in Table 4. In DBST modeling, the optimum ANFIS structure consists of three Gbellmf for AGE input and two Gbellmf for CESAL input, and six rules, and being trained for 335 epochs. While, for AC modeling, the optimum ANFIS structure consists of three Gauss2mf for both AGE and YESAL, and nine rules, and being trained for 250 epochs to prevent overfitting. The constant MF type has been used for the output variable (*IRI*) for both DBST and AC models.

Table 4. The full description of the optimum ANFIS models for DBST and AC pavement sections.

Description	DBST	AC
No. of Inputs	2	2
No. of Outputs	1	1
No. of Training dataset	189	86
No. of Checking dataset	40	18
No. of Testing dataset	40	18
Input MF No.	3 (AGE) 2 (CESAL)	3 (AGE) 3 (YESAL)
MF Type—Inputs	Gbellmf	Gauss2mf
MF Type—Outputs	Constant	Constant
Rules No.	6	9
Optimum Epoch No.	335	250
Learning Algorism	Hybrid	Hybrid
RMSE—Training Data	0.357	0.355
RMSE—Checking Data	0.449	0.206
RMSE—Testing Data	0.363	0.320
RMSE—Overall Data	0.373	0.357

5. Result Analysis

Once each network was developed using a training dataset and checked, it was tested using the test dataset to ensure the good generalization ability of the trained network. Similar to the checking dataset, a test dataset is never used for training the network. Figures 14 and 15 show scatter plots of the measured and the predicted *IRI* values of DBST and AC pavement sections, respectively, using the ANFIS model for training, checking, testing, and all datasets.

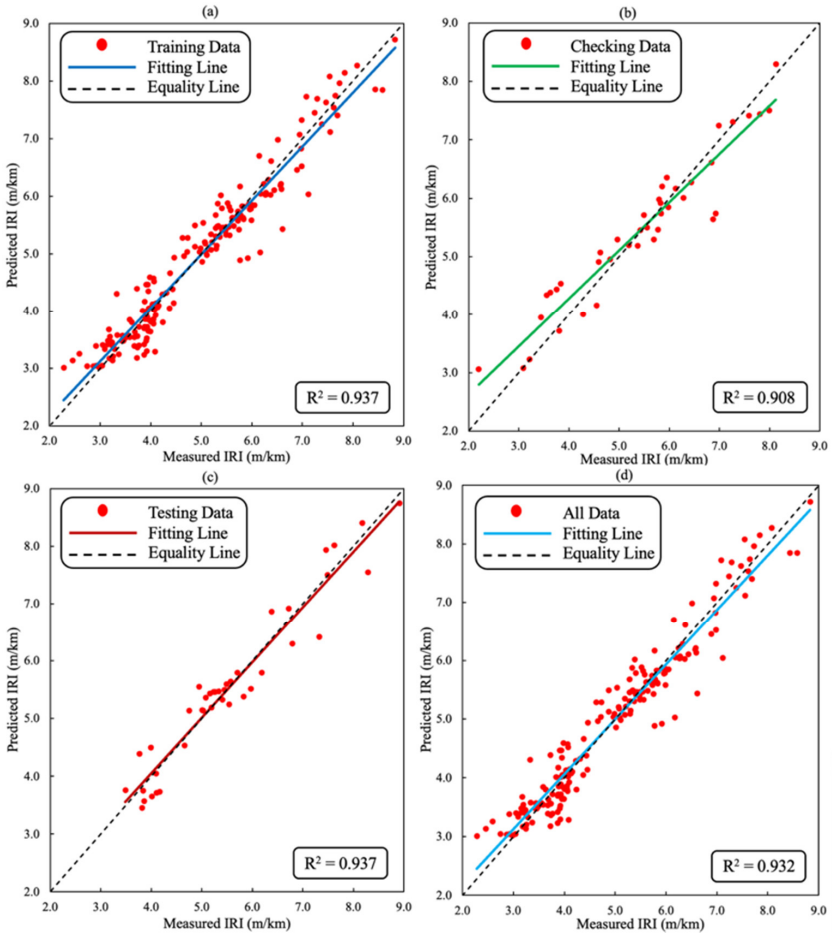

Figure 14. DBST regression analysis results between measured and predicted *IRI* values for the (**a**) training, (**b**) checking, (**c**) testing, and (**d**) all data.

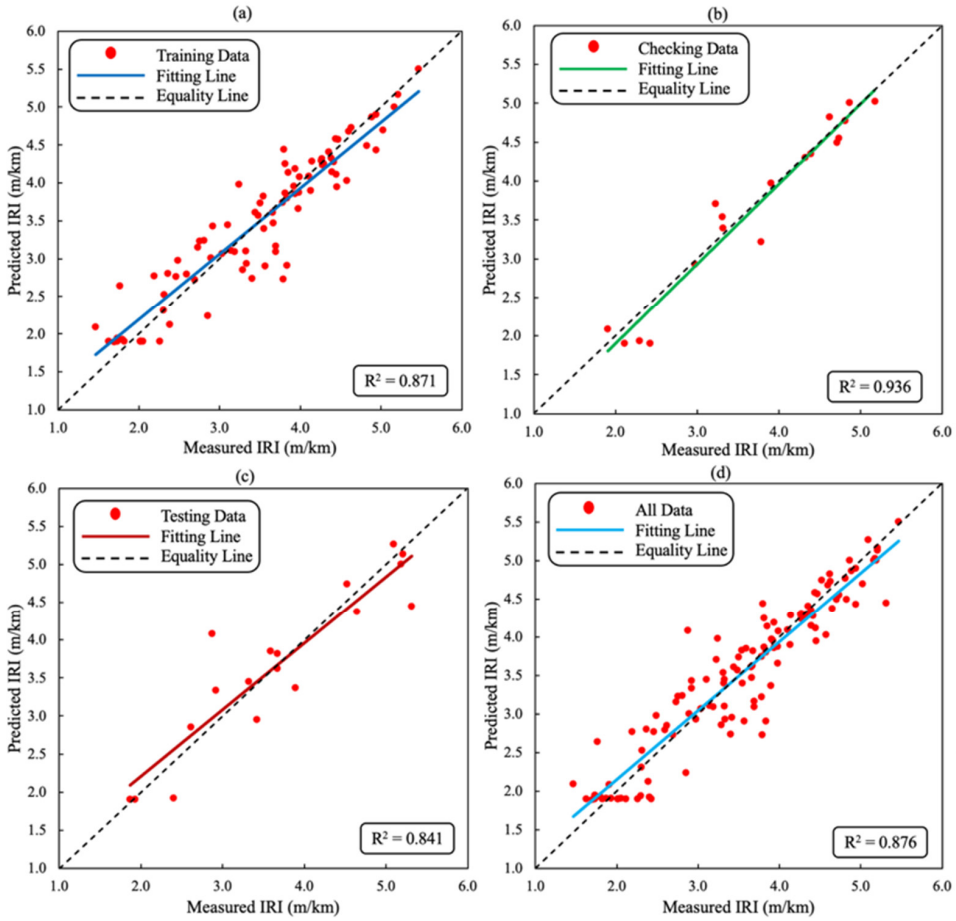

Figure 15. AC regression analysis results between measured and predicted *IRI* values for the (**a**) training, (**b**) checking, (**c**) testing, and (**d**) all data.

The figures showed a good distribution of data points around the equality line, indicating a highly accurate prediction of the developed models. The equality line is the target of the training activity. Moreover, the R^2, MAE, and RMSPE were calculated for training, checking, testing, and all datasets in DBST and AC models, as shown in Table 5.

Table 5. Performance of the DBST and the AC models of training, checking, testing, and all data.

Parameter	DBST Model				AC Model			
	Training	Checking	Testing	All	Training	Checking	Testing	All
n	189	40	40	269	86	18	18	122
R^2	0.937	0.908	0.937	0.932	0.871	0.936	0.841	0.876
MAE	0.269	0.335	0.298	0.283	0.267	0.264	0.439	0.266
RMSPE	8.163	10.722	6.861	8.421	12.730	9.039	13.485	12.374

The modeling results show that the developed models are very efficient in modeling the *IRI*. The values of R^2, MSA, and RMSPE for the DBST model were equal to 0.932, 0.283, and 8.421, respectively, meanwhile they were equal to 0.876, 0.266, and 12.374 for the AC model, considering all datasets. Larger values of R^2 and lower values of MAE/RMSPE suggest that a strong correlation exists between the predicted and the measured *IRI* values.

Besides statistical evaluation, the RE% test was also conducted to check and demonstrate the accuracy of the proposed models. RE% plots are shown in Figure 16 for the optimum ANFIS model developed for DBST and AC.

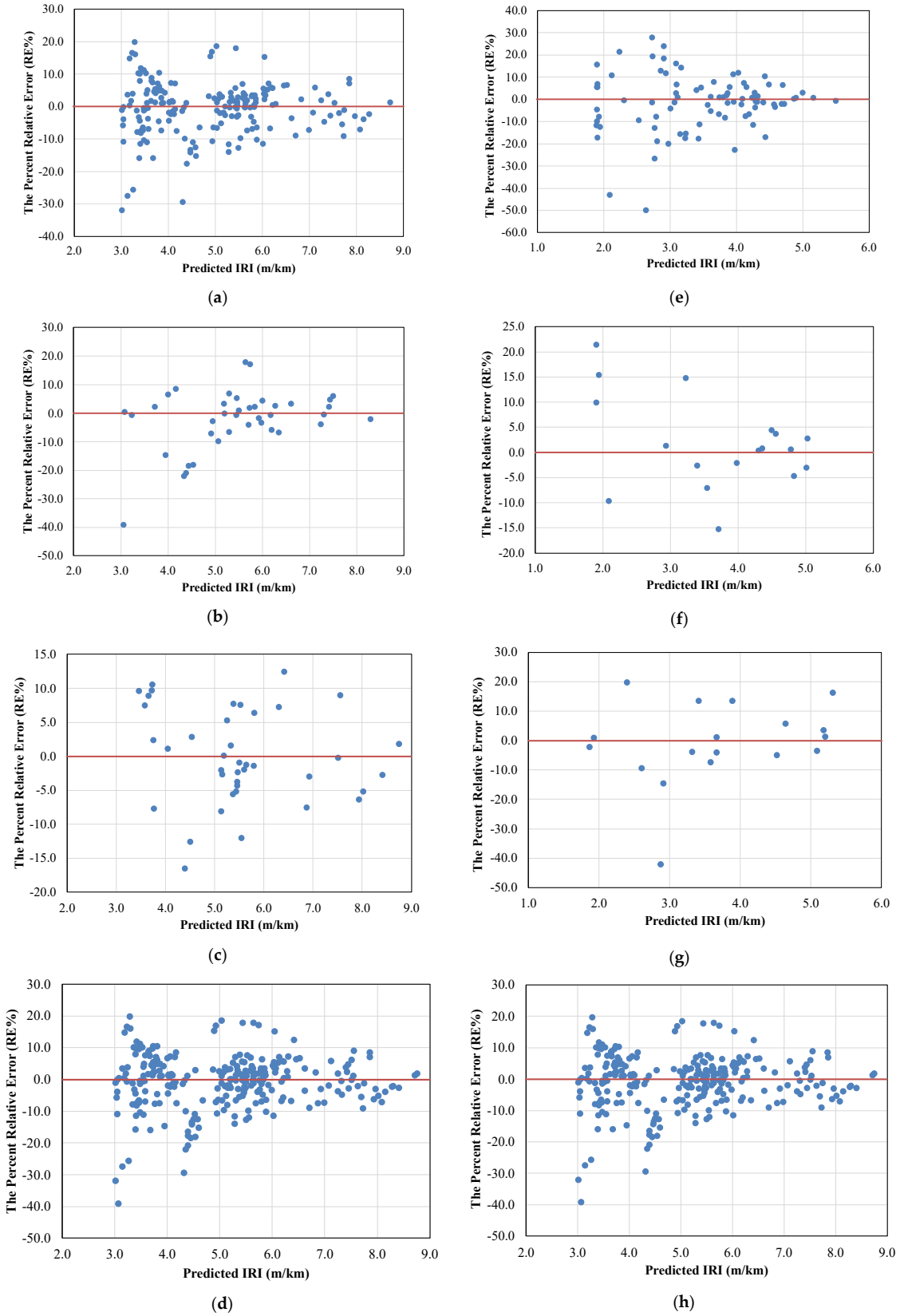

Figure 16. The RE% for the training, checking, testing, and overall datasets of DBST and AC models. (**a**) Training dataset for DBST Model, (**b**) Checking dataset for DBST Model, (**c**) Testing dataset for DBST Model, (**d**) Overall dataset for DBST Model, (**e**) Training dataset for AC Model, (**f**) Checking dataset for AC Model, (**g**) Checking dataset for AC Model, (**h**) Checking dataset for AC Model.

The results for both DBST and AC models show that most residual errors of the training, checking, testing, and overall datasets are mainly concentrated between +20% and −20%, describing the capacity of the developed ANFIS models for predicting the target output.

Moreover, the max RE% results are under 30% and −50%, which indicates that, up to a limited extent, the ANFIS models underestimated or overestimated the observed *IRI* values. The positive RE% results mean that the models underestimated the targeted *IRI* value ($IRI_{pred} < IRI_{act}$) by a maximum of 30%. In contrast, the negative RE% results indicate that the models overestimated the targeted *IRI* value ($IRI_{pred} > IRI_{act}$) by a maximum of 50%. Overall, the statistical results reveal that both ANFIS models have a good prediction ability, and their high R^2 values show their success in predicting the *IRI*.

The influence of input parameters on the output in the training phase of the ANFIS model is indicated by the 3D surface plots for DBST and AC models, as illustrated in Figure 17. The variation of *IRI* is plotted against AGE and CESAL in the DBST model and AGE and YESAL in the AC model.

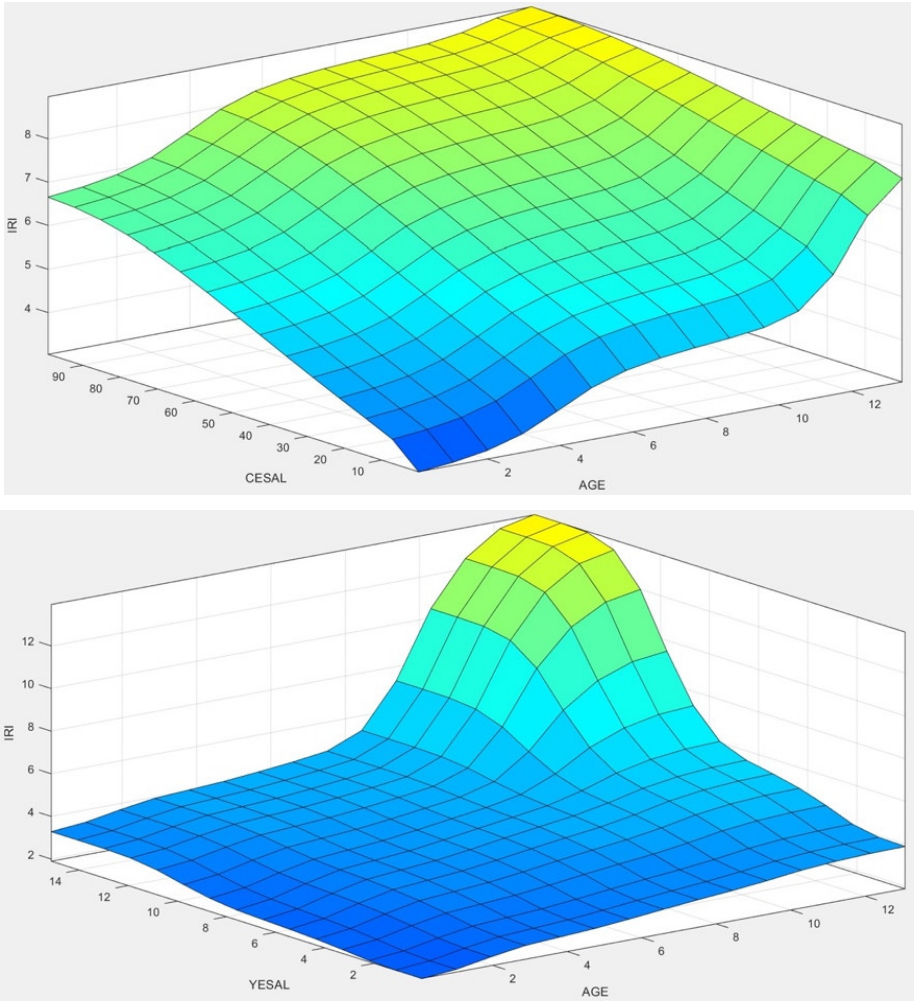

Figure 17. 3D surface plots for the effect of AGE and CESAL/YESAL on *IRI* for the (**a**) DBST model and (**b**) AC model.

The linearly increasing trend in Figure 17a can be observed for the *IRI* values with the increase in input variables (AGE and CESAL). Furthermore, a similar result can be seen in Figure 17b with a noticeable increase in the *IRI* values, especially with the increase in pavement AGE of more than eight years and more than 10×10^4 axle/lane in YESAL. The figure shows that the relationship between input variables (Age and CESAL or YESAL) and *IRI* is nonlinear. The increasing tendency of the *IRI* with the inputs variables agrees with

previous literature that *IRI* is directly related to pavement age and traffic loads. Therefore, this indicates the excellent identification capability of the ANFIS models.

6. Comparative Study

The proposed ANFIS models were compared statistically with the previously developed MLR models [32] for both DBST and AC pavement sections. R^2, MAE, and RMSPE were calculated for the ANFIS and MLR models using training datasets. From the results reported in Table 6, it can be observed that the ANFIS models for both BDST and AC pavement sections present high R^2 and low MAE and RMSPE values, although the goodness of fit statistics of the MLR models for both DBST and AC pavement sections are less efficient compared with those corresponding to ANFIS models.

Table 6. Comparison of the goodness of fit statistics for the ANFIS and the MLR models.

Parameter	DBST Model		AC Model	
	ANFIS	MLR	ANFIS	MLR
n	189	215	86	98
R^2	0.937	0.892	0.871	0.847
MAE	0.269	0.336	0.267	0.314
RMSPE	8.163	9.626	12.730	12.186

7. Study Limitations and Recommendations for Future Work

Despite the significant influence of the environmental factors, subgrade soil properties, pavement structural capacity, and IRI_0 value on the progression of the unevenness [28,52–54], an assessment of the effect of those factors on *IRI* progression was not possible since the Laos PMS database does not have any information regarding those variables. So, the effect of those variables on *IRI* progression will be further studied.

8. Conclusions

This study utilized the ANFIS approach to develop *IRI* prediction models for DBST and AC pavement sections for Laos NRN. ANFIS approach is chosen mainly because of its good capability of learning, constructing, and classifying the input-target data [22,31]. The findings presented in this paper are obtained from 269 and 122 observations covering 1850 km of DBST NRN and 718 km of AC NRN.

In DBST modeling, the optimum ANFIS structure consists of three Gbellmf for AGE input and two Gbellmf for CESAL input, six fuzzy rules, and being trained for 335 epochs where the checking error is equal to 0.493. While, for AC modeling, the optimum ANFIS structure consists of three Gauss2mf for both AGE and YESAL, nine fuzzy rules, and being trained for 250 epochs to prevent overfitting where the checking error is equal to 0.264. The constant MF type has been used for the output variable (*IRI*) for both DBST and AC models.

Predicted *IRI* values affirmed the effectiveness of the proposed ANFIS models for predicting the *IRI* as a function of pavement age and traffic loads (CESAL or YESAL). The values of R^2, MSA, and RMSPE for the DBST model were equal to 0.932, 0.283, and 8.421, respectively, meanwhile they were equal to 0.876, 0.266, and 12.374 for the AC model, considering all datasets. Furthermore, results revealed that ANFIS models yielded higher prediction accuracy than MLR models previously developed under the same conditions. Eventually, proposed ANFIS models can assist authorities in predicting pavement conditions in the future and, as a result, estimating MR needs and setting priorities among projects under restricted funds.

Author Contributions: Investigation, methodology, data curation, formal analysis, and writing—original draft preparation, M.G.; conceptualization, resources, validation, writing—review and editing, and supervision, T.N., S.N. and K.T. All authors have read and agreed to the published version of the manuscript.

Funding: This research was funded by JICA, Road Asset Management Project, Grant No. (D1810488).

Institutional Review Board Statement: Not applicable.

Informed Consent Statement: Not applicable.

Data Availability Statement: The data presented in this study are available on request from the corresponding author. The data are not publicly available due to privacy restrictions.

Acknowledgments: The authors would like to express their gratitude to the Laos Public Works and Transport Institute (PTI), Ministry of Public Work and Transport, for granting permission to use the Laos PMS database for developing the pavement roughness models.

Conflicts of Interest: The authors declare no conflict of interest.

References

1. *AASTHO Pavement Management Guide*, 2nd ed.; AASHTO: Washington, WA, USA, 2012.
2. Pérez-Acebo, H.; Linares-Unamunzaga, A.; Rojí, E.; Gonzalo-Orden, H. IRI performance models for flexible pavements in two-lane roads until first maintenance and/or rehabilitation work. *Coatings* **2020**, *10*, 97. [CrossRef]
3. Loprencipe, G.; Zoccali, P. Ride quality due to road surface irregularities: Comparison of different methods applied on a set of real road profiles. *Coatings* **2017**, *7*, 59. [CrossRef]
4. ARA. *Guide for Mechanistic-Empirical Design of New and Rehabiltated Pavement Structures*; Appendix OO-1: Background and Preliminary Smoothness Prediction Models for Flexible Pavements; National Cooperative Highway Research Program: Champaign, IL, USA, 2001.
5. Pérez-Acebo, H.; Bejan, S.; Gonzalo-Orden, H. Transition Probability Matrices for Flexible Pavement Deterioration Models with Half-Year Cycle Time. *Int. J. Civ. Eng.* **2018**, *16*, 1045–1056. [CrossRef]
6. Kirbaş, U. IRI sensitivity to the influence of surface distress on flexible pavements. *Coatings* **2018**, *8*, 271. [CrossRef]
7. Múčka, P. International Roughness Index specifications around the world. *Road Mater. Pavement Des.* **2017**, *18*, 929–965. [CrossRef]
8. Zeiada, W.; Hamad, K.; Omar, M.; Underwood, B.S.; Khalil, M.A.; Karzad, A.S. Investigation and modelling of asphalt pavement performance in cold regions. *Int. J. Pavement Eng.* **2019**, *20*, 986–997. [CrossRef]
9. Marcelino, P.; de Lurdes Antunes, M.; Fortunato, E.; Gomes, M.C. Machine learning approach for pavement performance prediction. *Int. J. Pavement Eng.* **2021**, *22*, 341–354. [CrossRef]
10. Chai, G.; Akli, O.; Asmaniza, A.; Singh, M.; Chong, C.L. Calibration of HDM Model for the North South Expressway in Malaysia. In Proceedings of the 6th International Conference on Managing Pavements, Brisbane, QLD, Australia, 19–24 October 2004; pp. 1–10.
11. Yogesh, U.S.; Jain, S.S.; Devesh, T. Adaptation of HDM-4 Tool for Strategic Analysis of Urban Roads Network. *Transp. Res. Procedia* **2016**, *17*, 71–80. [CrossRef]
12. Bennett, C.R.; Paterson, W.D.O. A Guide to Calibration and Adaptation. In *HDM 4—Highway Developmenet & Management Series*; TRL: Paris, France, 2000; Volume 5.
13. Braga, A.; Čygas, D. Adaptation of pavement deterioration models to lithuanian automobile roads. *J. Civ. Eng. Manag.* **2002**, *8*, 214–220. [CrossRef]
14. Ognjenovic, S.; Krakutovski, Z.; Vatin, N. Calibration of the crack initiation model in HDM 4 on the highways and primary urban streets network in Macedonia. *Procedia Eng.* **2015**, *117*, 559–567. [CrossRef]
15. Jain, S.S.; Aggarwal, S.; Parida, M. HDM-4 pavement deterioration models for Indian national highway network. *J. Transp. Eng.* **2005**, *131*, 623–631. [CrossRef]
16. Han, D.; Kobayashi, K.; Do, M. Improved calibration for HDM-4 implementation: A lesson from Korean experiences. *Jsce* **2009**, *4*. Available online: http://library.jsce.or.jp/jsce/open/00039/200911_no40/pdf/84.pdf (accessed on 22 January 2022).
17. Han, D.; Kobayashi, K.; Do, M. Section-based multifunctional calibration method for pavement deterioration forecasting model. *KSCE J. Civ. Eng.* **2013**, *17*, 386–394. [CrossRef]
18. La Torre, F.; Domenichini, L.; Darter, M.I. Roughness prediction model based on the artificial neural network approach. In Proceedings of the Fourth International Conference on Managing Pavements, Durban, South Africa, 17–21 May 1998; Volume 2.
19. Lin, J.-D.; Yau, J.-T.; Hsiao, L.-H. Correlation analysis between international roughness index (IRI) and pavement distress by neural network. In Proceedings of the 82nd Annual Meeting of the Transportation Research Board, Washington, DC, USA, 12–16 January 2003; pp. 12–16.
20. Hossain, M.; Gopisetti, L.S.P.; Miah, M.S. Artificial neural network modelling to predict international roughness index of rigid pavements. *Int. J. Pavement Res. Technol.* **2020**, *13*, 229–239. [CrossRef]
21. Kaloop, M.; El-Badawy, S.; Ahn, J.; Sim, H.-B.; Hu, J.; Abd El-Hakim, R. A Hybrid Wavelet-Optimally-Pruned Extreme Learning Machine Model for the Estimation of International Roughness Index of Rigid Pavements. *Int. J. Pavement Eng.* **2020**, *23*, 1–15. [CrossRef]

22. Nguyen, H.-L.; Pham, B.T.; Son, L.H.; Thang, N.T.; Ly, H.-B.; Le, T.-T.; Ho, L.S.; Le, T.-H.; Tien Bui, D. Adaptive network based fuzzy inference system with meta-heuristic optimizations for international roughness index prediction. *Appl. Sci.* **2019**, *9*, 4715. [CrossRef]
23. Choi, J.H.; Adams, T.M.; Bahia, H.U. Pavement roughness modeling using back-propagation neural networks. *Comput. Civ. Infrastruct. Eng.* **2004**, *19*, 295–303. [CrossRef]
24. Teomete, E.; Bayrak, M.B.; Agarwal, M. Use of Artificial Neural Networks for Predicting Rigid Pavement Roughness. In Proceedings of the 2004 Transportation Scholars ConferenceIowa State University, Ames, IA, USA, 19 November 2004.
25. Chou, S.F.; Pellinen, T.K. Assessment of construction smoothness specification pay factor limits using artificial neural network modeling. *J. Transp. Eng.* **2005**, *131*, 563–570. [CrossRef]
26. Abd El-Hakim, R.; El-Badawy, S. International roughness index prediction for rigid pavements: An artificial neural network application. *Adv. Mater. Res.* **2013**, *723*, 854–860. [CrossRef]
27. Ziari, H.; Sobhani, J.; Ayoubinejad, J.; Hartmann, T. Prediction of IRI in short and long terms for flexible pavements: ANN and GMDH methods. *Int. J. Pavement Eng.* **2015**, *17*, 776–788. [CrossRef]
28. Mazari, M.; Rodriguez, D.D. Prediction of pavement roughness using a hybrid gene expression programming-neural network technique. *J. Traffic Transp. Eng.* **2016**, *3*, 448–455. [CrossRef]
29. Abdelaziz, N.; Abd El-Hakim, R.T.; El-Badawy, S.M.; Afify, H.A. International roughness index prediction model for flexible pavements. *Int. J. Pavement Eng.* **2020**, *21*, 88–99. [CrossRef]
30. Georgiou, P.; Plati, C.; Loizos, A. Soft Computing Models to Predict Pavement Roughness: A Comparative Study. *Adv. Civ. Eng.* **2018**, *2018*, 5939806. [CrossRef]
31. Terzi, S. Modeling for pavement roughness using the ANFIS approach. *Adv. Eng. Softw.* **2013**, *57*, 59–64. [CrossRef]
32. Gharieb, M.; Nishikawa, T. Development of Roughness Prediction Models for Laos National Road Network. *CivilEng* **2021**, *2*, 158–173. [CrossRef]
33. Laos Ministry of Public Works and Transport, Department of Roads. *Summary of Road Network Statistics Year*; Laos Ministry of Public Works and Transport: Vientiane, Laos, 2020.
34. Tarno; Rusgiyono, A.; Sugito. Adaptive Neuro Fuzzy Inference System (ANFIS) approach for modeling paddy production data in Central Java. *J. Phys. Conf. Ser.* **2019**, *1217*, 012083. [CrossRef]
35. Naresh, C.; Bose, P.S.C.; Rao, C.S.P. Artificial neural networks and adaptive neuro-fuzzy models for predicting WEDM machining responses of Nitinol alloy: Comparative study. *SN Appl. Sci.* **2020**, *2*, 1–23. [CrossRef]
36. Jang, J.-S. ANFIS: Adaptive-network-based fuzzy inference system. *IEEE Trans. Syst. Man. Cybern.* **1993**, *23*, 665–685. [CrossRef]
37. Jang, J.-S.R.; Sun, C.-T.; Mizutani, E. Neuro-fuzzy and soft computing-a computational approach to learning and machine intelligence [Book Review]. *IEEE Trans. Automat. Contr.* **1997**, *42*, 1482–1484. [CrossRef]
38. Zadeh, L.A. Fuzzy sets. In *Fuzzy Sets, Fuzzy Logic, and Fuzzy Systems: Selected Papers by Lotfi A Zadeh*; World Scientific: River Edge, NJ, USA, 1996; pp. 394–432.
39. Çekmiş, A.; Hacıhasanoğlu, I.; Ostwald, M.J. A computational model for accommodating spatial uncertainty: Predicting inhabitation patterns in open-planned spaces. *Build. Environ.* **2014**, *73*, 115–126. [CrossRef]
40. Sivanandam, S.N.; Sumathi, S.; Deepa, S.N. Fuzzy rule-based system. In *Introduction to Fuzzy Logic Using Matlab*; Springer: Berlin, Germany, 2007; pp. 113–149.
41. Cabalar, A.F.; Cevik, A.; Gokceoglu, C. Some applications of adaptive neuro-fuzzy inference system (ANFIS) in geotechnical engineering. *Comput. Geotech.* **2012**, *40*, 14–33. [CrossRef]
42. Singh, R.; Kainthola, A.; Singh, T.N. Estimation of elastic constant of rocks using an ANFIS approach. *Appl. Soft Comput.* **2012**, *12*, 40–45. [CrossRef]
43. Takagi, T.; Sugeno, M. Fuzzy identification of systems and its applications to modeling and control. *IEEE Trans. Syst. Man. Cybern.* **1985**, *SMC-15*, 116–132. [CrossRef]
44. Finol, J.; Guo, Y.K.; Jing, X.D. A rule based fuzzy model for the prediction of petrophysical rock parameters. *J. Pet. Sci. Eng.* **2001**, *29*, 97–113. [CrossRef]
45. Manual, M. *Fuzzy Logic Toolbox^{TM} User's Guide*; MathWorks: Natick, MA, USA, 2009.
46. Yaseen, Z.M.; Ebtehaj, I.; Bonakdari, H.; Deo, R.C.; Mehr, A.D.; Mohtar, W.H.M.W.; Diop, L.; El-Shafie, A.; Singh, V.P. Novel approach for streamflow forecasting using a hybrid ANFIS-FFA model. *J. Hydrol.* **2017**, *554*, 263–276. [CrossRef]
47. Shah, M.I.; Abunama, T.; Javed, M.F.; Bux, F.; Aldrees, A.; Tariq, M.A.U.R.; Mosavi, A. Modeling Surface Water Quality Using the Adaptive Neuro-Fuzzy Inference System Aided by Input Optimization. *Sustainability* **2021**, *13*, 4576. [CrossRef]
48. Vasileva-Stojanovska, T.; Vasileva, M.; Malinovski, T.; Trajkovik, V. An ANFIS model of quality of experience prediction in education. *Appl. Soft Comput.* **2015**, *34*, 129–138. [CrossRef]
49. Tiwari, S.; Babbar, R.; Kaur, G. Performance evaluation of two ANFIS models for predicting water quality Index of River Satluj (India). *Adv. Civ. Eng.* **2018**, *2018*, 8971079. [CrossRef]
50. Hamdi; Hadiwardoyo, S.P.; Correia, A.G.; Pereira, P.; Cortez, P. Prediction of surface distress using neural networks. *AIP Conf. Proc.* **2017**, *1855*, 040006. [CrossRef]
51. Al-Hmouz, A.; Shen, J.; Al-Hmouz, R.; Yan, J. Modeling and simulation of an adaptive neuro-fuzzy inference system (ANFIS) for mobile learning. *IEEE Trans. Learn. Technol.* **2011**, *5*, 226–237. [CrossRef]

52. Odoki, J.B.; Kerali, G.R.H. Volume Four: Analytical Framework and Model Descriptions. In *Highway Development and Management Model HDM-4 (Version 1.2)*; TRL: Paris, France, 2001.
53. Sandra, A.K.; Sarkar, A.K. Development of a model for estimating International Roughness Index from pavement distresses. *Int. J. Pavement Eng.* **2013**, *14*, 715–724. [CrossRef]
54. Makendran, C.; Murugasan, R.; Velmurugan, S. Performance prediction modelling for flexible pavement on low volume roads using multiple linear regression analysis. *J. Appl. Math.* **2015**, *2015*, 192485. [CrossRef]